Graphene Oxide Nanofilm and Chicken Embryo Extract Decrease the Invasiveness of HepG2 Liver Cancer Cells.

Malwina Sosnowska
Szkola Glowna Gospodarstwa Wiejskiego
Marta Kutwin
Szkola Glowna Gospodarstwa Wiejskiego
Barbara Strojny
Szkola Glowna Gospodarstwa Wiejskiego
Piotr Koczoń
Szkola Glowna Gospodarstwa Wiejskiego
Jarosław Szczepaniak
Szkola Glowna Gospodarstwa Wiejskiego
Jaśmina Bałaban
Szkola Glowna Gospodarstwa Wiejskiego
Karolina Daniluk
Szkola Glowna Gospodarstwa Wiejskiego
Sławomir Jaworski
Szkola Glowna Gospodarstwa Wiejskiego
André Chwalibog
Kobenhavns Universitet
Wiesław Bielawski
Szkola Glowna Gospodarstwa Wiejskiego
Ewa Sawosz (ewa_sawosz_chwalibog@sggw.edu.pl)
Szkola Glowna Gospodarstwa Wiejskiego https://orcid.org/0000-0002-0016-4721

Research

Keywords: adhesion, cell cycle, embryo liver extract, extracellular matrix, graphene oxide nanofilm, liver cancer, proliferation

Posted Date: August 11th, 2020

DOI: https://doi.org/10.21203/rs.3.rs-53244/v1

Version of Record: A version of this preprint was published at Cancer Nanotechnology on January 6th, 2021. See the published version at https://doi.org/10.1186/s12645-020-00073-5.

Abstract

Background: The extracellular matrix (ECM) is a mosaic of various structural and functional proteins that cooperate with the cell, regulate adhesion, and consequently manage its further fate. Liver destruction is accompanied by a disruption of the physicochemical properties of the ECM which deregulates the cell-ECM interaction and can lead to uncontrolled proliferation and neoplastic transformation of cells. Therefore, it can be assumed that ECM modification and restoration of its characteristics for healthy tissue may counteract uncontrolled cell proliferation. The purpose of the presented research model was to optimise the physical characteristics of ECM by introducing a graphene oxide plane/nanofilm (nfGO) and enriching the cell environment with potentially missing proteins by adding a functional protein cocktail (chicken embryo liver extract) and determine the impact of these factors on cell-ECM cooperation and its consequences on adhesion, proliferation, and cell phase, which are factors of the invasiveness of cancer cells.

Results: Experiments were performed with non-cancer HS-5 cells and liver cancer cells HepG2 and C3A. The cells were divided into four groups; (1) control, (2) cultured on GO nanofilm, (3) cultured with the addition of chicken embryo liver extract (CELE) to the medium and (4) cultured on the GO nanofilm with the addition of CELE. CELE contained 1735 proteins; the top 57 of these proteins have been presented. The use of GO nanofilm as well as CELE and nfGO + CELE reduced the proliferation of HepG2 cancer cells to the greatest extent; this is in contrast to non-cancer cells and also to C3A cancer cells. Furthermore, the combined use of the CELE protein cocktail and GO substrate effectively resulted in a decrease in the population of HepG2 cells in the G0/G1 phase and an increase of the population in G2/M. Molecular analysis of HepG2 cancer cells also showed an increase in the expression of genes responsible for adhesion such as *fak* (*focal adhesion kinase*), *e-cadherin,* and *n-cadherin* and a decrease in *β-catenin*, which is considered a proto-oncogen.

Conclusions: Studies have shown that both the GO surface structure on which the cells are grown as well as the presence of a multi-component natural cocktail of regulatory proteins, can modify the expression of integrins, increase adhesion and, as a consequence, proliferation and the cell cycle - entering the resting phase. For the first time, it has been documented that hepatic cancer cells of the HepG2 line under the influence of stimuli derived from mimic ECM (graphene oxide) in interaction with a unique protein complex derived from chicken liver embryo decreased of the invasiveness of cancer cells.

1. Background

Hepatocellular carcinoma (HCC) is aggressive, fast growing, and the second cause of cancer death in the world. The key reason for the development of this cancer is liver fibrosis and cirrhosis as a consequence of chronic liver injury [1] caused by inflammation induced through, inter alia, virus infections (HCV and HBV) [2]. The inflammatory process is coupled with deepening degradation of the extracellular matrix (ECM). It is also known that from the processes occurring in the cell, its behaviour and fate depend decisively on its environment and above all on the ECM. Disrupted ECM may cause neoplastic

transformation of cells, tumour progression, and metastasis [3]. On the other hand, in the inflammatory process, tumour associated cells possess impaired secretion of matrix proteins, which leads to overproduction and reorganisation of ECM components. Collagen fibres become thin and branched, and, as a consequence, increase ECM stiffness in fibrotic tissue [2, 4, 5, 6]. The level of ECM stiffness affects cell proliferation and determines migration, adhesion, and, consequently, the phenotype of the cell. What's more, different tissues have ECM stiffness precisely characteristic and optimal for their proper development [7]. Paradoxically, ECM degradation can lead to cancer cell transformation, and the resulting cancer cells stimulate the ECM reorganisation (stiffening) process creating a kind of feedback. Inhibiting this feedback is the key to stopping and possibly treating cancer.

ECM is the physical support for cells recognised by their receptors – integrins. Integrins sense ECM stiffness and transfer signals towards focal adhesion kinase (FAK) cytoskeleton and nucleus [5]. Thus, mechanical signals from the cell environment regulate the expression of genes, including genes involved in cell metabolism and in ECM degradation and synthesis [8]. Cancer cells have a reprogrammed metabolism to affect lactic acid synthesis from pyruvate under aerobic conditions [9]. Acidification of the cell environment ensures activation of ECM remodelling enzymes, which leads to pathology in stiffness, elasticity, fibre density, and roughness of ECM [10]. Impaired signal transduction to cells promotes relaxation of cell-cell connections. Thus, cooperation between ECM and cancer cells contributes to irreversible liver fibrosis – cirrhosis [11].

ECM comprises over 300 proteins, 200 glycoproteins, and 30 proteoglycans that create an extremely complicated and dynamic structure [8]. Loss of several components from the functional and structural protein pool may disrupt their synergistic or antagonistic activity and zonal distribution of ECM components. For example, HCC is associated with a decrease in the amount of elastic fibres, microfibrils (tenascin), proteoglycans 4, and FACIT collagens (Col14A, Col16A). Furthermore, removal of the basement membrane, containing laminins and collagen type 4, facilitates the transition to vessels and invasion [12, 13].

The key strategy for creating artificial ECM is by reconstruction of the physicochemical and mechanical properties of healthy tissue. Carbon allotropes, especially graphene oxide (GO), can create promising nanofilms for cell growth due to their self-organization and functionalisation ability [14]. The large surface area and hydrophilic properties of GO promote anchoring and successful functionalisation with various molecules [15]. Mechanical signalling, derived from a nanofilm formed by nanoparticles of allotropic forms of carbon and showing natural roughness, determines the affinity and adhesion of cells [15, 16, 17]. The biocompatibility and unique characteristics of GO, in particular flexibility, stability, hydrophilic and nano-dimensions, suggest using it as a biomimic ECM. Therefore, GO, as a nanofilm supporting degraded ECM, could optimise its characteristics and be a source of proper mechano-signalling for the cell. However, stopping feedback also requires the supply of a wide spectrum of non-specific proteins, especially those forming the ECM or ECM-cell interface, whose production in the process of carcinogenesis has been inhibited or impaired, especially the production of ligands for integrins.

The mixture of the total embryo proteins has a broad and universal spectrum of action that is useful in plastic and reconstructive surgery [18]. The embryonic mosaic of the cell microenvironment is used to grow stem cells as an alternative to serum [19]. In *in vitro* conditions, serum elements provide cell adhesion to a plate and prevent the loss of epithelial characteristics in cells [20]. A cocktail of growth factors, despite their wound healing function, prevents uncontrolled proliferation of tumour cells by supplementation with missing ECM biomolecules and expression of regulating suppressor genes [21]. It seems that a natural mixture of proteins derived from an embryonic liver extract of another species should be a unique source of non-specific factors with multiple functions. Thus, a combination of two signals, mechanotransduction from a graphene surface and a molecular signal from the protein cocktail, could inhibit tumour cell-ECM feedback, restore proper cell contact with the environment, inhibit proliferation, and increase the population of cells in the G2/M phase of the cycle.

The objective of this study was to evaluate whether GO nanofilm (nfGO), as a biomimic ECM equivalent, and CELE, as a source of essential and missing proteins in tumour tissue, reduce activity characteristic of liver cancer cells and restore the properties of normal cells, particularly in terms of adhesion, proliferation and cell cycle.

2. Results

2.1. Characterisation of GO

2.1.1. Characterisation of GO flakes

GO, observed with TEM, created single-layered, slightly wrinkled flakes that ranged from 100 nm to 2.9 μm in size (Fig. 1A). GO suspended in ultra-pure water at a concentration of 50 mg/L showed high stability and no tendency for agglomeration. The zeta potential of the GO was − 27.5 mV.

Chemical groups present on GO were identified by the Fourier transform infrared (FTIR) method (Fig. 1B). The most characteristic features of the nanomaterial spectra were the intense, broad bands at 3457 cm^{-1}, which correspond to O–H stretching rotations. The O–H stretch together with the shoulder bands located at 1728 cm^{-1} confirm the presence of at least some oxygen attached to carbon. We observed four characteristic bands generated by C–H stretching at approximately 2959–2642 cm^{-1}. Bands generated by aromatic ring carbon–carbon double bonds were present at 1621 cm^{-1} in the GO spectra [22]. This location corresponds to the sp^2 character of GO [23]. The presence of only seven bands in the spectrum of the GO material confirms its simple composition of only three atoms (carbon, oxygen, and hydrogen).

2.1.2. Characterisation of GO nanofilm

GO nanofilm was formed by applying a GO colloid to the bottom of a plastic cell culture plate and drying it. The topography of the surface of the plastic culture plate *vs* the nanofilm GO coated plate was

determined by atomic force microscopy (AFM) (Fig. 2A,B). It can be seen that the morphology differed significantly between plastic and plastic coated with GO surfaces. The average roughness of the uncoated surface was Ra = 1.5 nm (Fig. 2A) and the roughness of the coated surface was Ra = 9.8 nm (Fig. 2B). Moreover, the maximum height of the roughness of the nfGO coated plate was four times greater than the uncoated culture plate. Some dense, transverse inequalities of GO were seen, corresponding to flakes arrangement. In summary, the average roughness of the surface increased about six times but was still in the nanometric range.

The hydrophilicity of the surface covered with nanofilm GO *vs* the polystyrene surface was measured. Generally, the contact surface of a water droplet on the nfGO was higher than on the uncoated plate (Fig. 2C). As shown in Fig. 2D, the area of the water droplet was increased about two times on the modified surface compared to the control; thus, the hydrophilicity of the surface increased after coating with GO.

2.2. Protein composition of the liver extract

1735 proteins were identified in the CELE by mass spectrometry analysis. The exact formulation of these proteins has been registered in PRoteomics IDentifications Database under PXD015146 [24]. The functions and scope of activity of the identified proteins were determined on the basis of the UniProt database, and on this basis 57 key proteins were selected that could be involved in adhesion, ECM organisation, migration, epithelial-mesenchymal transition (EMT), proliferation, cell cycle, and apoptosis of cancer cells of the liver (Table 1).

Table 1
The top 57 proteins from the chicken liver extract divided into functional activities according to UniProt database, including the name of the gene and the molecular mass of the protein (kDa)

No.	Gene name	Protein name	Molecular mass [kDa]
ADHESION			
1	TJP2	Tight junction protein ZO-2	130.7
2	LARP1	La-related protein 1	118.6
3	CDH1	Cadherin-1	97.8
4	CD2AP	CD2-associated protein	71.2
5	tr|A0A1D5PRE3|A0A1D5PRE3_CHICK	N-myc downstream regulated	39.0
6	EPCAM	Epithelial cell adhesion molecule	34.4
7	MTDH	Metadherin	14.2
8	BSG	Basigin	Few isoforms
ECM ORGANISATION			
9	LAMA1	Laminin subunit alpha-1	339.1
10	COL12A1	Collagen alpha-1(XII) chain	333.5
11	FN1	Fibronectin	273.2
12	COL5A1	Collagen alpha-1(V) chain	184.2
13	LAMC1	Laminin subunit gamma-1	176.5
14	PEPD	Xaa-Pro dipeptidase	55.1
15	VTN	Vitronectin	51.7
16	PRDX4	Peroxiredoxin-4	29.6
MIGRATION AND EMT			
17	PTPN23	Tyrosine-protein phosphatase non-receptor type 23	179.0
18	FAM98A	Protein FAM98A	58.6
19	TWF1	Twinfilin-1	55.2
20	MGLL	Monoglyceride lipase	33.3
21	TPM1	Tropomyosin alpha-1 chain	32.8

No.	Gene name	Protein name	Molecular mass [kDa]
22	PBLD	Phenazine biosynthesis-like domain-containing protein	32.2
23	ADI1	1,2-dihydroxy-3-keto-5-methylthiopentene dioxygenase	21.7
PROLIFERATION AND CELL CYCLE			
24	GOLGA2	Golgin subfamily A member 2	140.1
25	MOV10	Putative helicase MOV-10	109.1
26	ASMTL	Probable bifunctional dTTP/UTP pyrophosphatase/methyltransferase protein	70.2
27	RPA1	Replication protein A 70 kDa DNA-binding subunit	68.0
28	ARID3A	AT-rich interactive domain-containing protein 3A	67.4
29	RIC8B	Guanine Nucleotide Exchange Factor B	60.5
30	CERS2	Ceramide synthase 2	55.1
31	KRT18	Keratin, type I cytoskeletal 18	46.9
32	MRPS27	28S ribosomal protein S27, mitochondrial	46.7
33	TARDBP	DNA-binding protein 43	44.6
34	CA9	Carbonic anhydrase 9	43.8
35	DRG1	Developmentally regulated GTP-binding protein 1	40.5
36	SLC35F6	Solute carrier family 35 member F6	40.2
37	AIMP2	Aminoacyl tRNA synthase complex-interacting multifunctional protein 2	34.5
38	FBXO6	F-box only protein 6	30.7
39	HPGD	15-hydroxyprostaglandin dehydrogenase [NAD(+)]	29.0
40	PSMD9	26S proteasome non-ATPase regulatory subunit 9	22.7
41	NIT2	Nitrilase NIT2	22.1
42	DYNLL1	Dynein light chain	10.3

No.	Gene name	Protein name	Molecular mass [kDa]
APOPTOSIS			
43	HTT	Huntingtin	344.0
44	PARP1	Poly [ADP-ribose] polymerase	113.1
45	DNMT3A	DNA (cytosine-5)-methyltransferase 3A	99.0
46	ATAD3A	ATPase family AAA domain-containing protein 3A	67.2
47	SGPL1	Sphingosine-1-phosphate lyase 1	61.1
48	CTSC	Dipeptidyl peptidase 1	59.4
49	FKBP8	Peptidylprolyl isomerase	44.3
50	AIFM2	Apoptosis-inducing factor 2	40.6
51	APIP	Methylthioribulose-1-phosphate dehydratase	26.8
52	PDCD10	Programmed cell death protein 10	24.7
53	ENDOG	Endonuclease G, mitochondrial	22.2
54	FAM162A	Protein FAM162A	17.1
55	HIGD1A	HIG1 domain family member 1A, mitochondrial	10.7
56	DYNLL1	Dynein light chain	10.3
57	NQO1	NAD(P)H dehydrogenase [quinone] 1	Few isoforms

2.3. Influence of nfGO and CELE on cell morphology

The morphological picture of non-tumour HS-5 cells after 48 h of incubation on GO nanofilm, with the addition of CELE and using both factors, did not indicate pathological changes, however, some differences could be found (Fig. 3). Cells growing on the nfGO were extended and possessed large cell bodies, long protrusions, and distinct lamellipodia. Cell clusters and high cell-cell adhesion were observed on the nfGO (Fig. 3B). The CELE induced severe morphological changes in HS-5 cells, such as elongation of filopodia, reduction of cell bodies (shrunken forms), and formation of small clusters (pieces of extract) (Fig. 3C). In the nfGO + CELE group, the HS-5 cell size was reduced and no tendency of cells to form clusters was observed (Fig. 3D).

HepG2 and C3A liver tumour cells form natural clusters as observed in the experiment with the control groups (Fig. 4A, Fig. 5A). After 48 h of culture, HepG2 cancer cells were also not pathologically altered

due to surface modification with GO nanofilm and CELE addition. Moreover, none of the experimental factors significantly changed their morphology (Fig. 4). Although it was observed that the cells were willingly located on the GO coated surface, they appeared to be more shrunken. The CELE additive to the cells caused some loosening of cell clusters. In the nfGO + CELE group there were more cells not associated in clusters but migrating outside the clusters.

C3A cells also did not undergo pathological changes under the influence of experimental factors (Fig. 5). C3A cells were visible on the GO surface as well as outside it. Under the influence of CELE addition, a number of cells could be seen separated from clusters. In the nfGO + CELE group, a greater number of individual cells that migrated outside of the clusters was observed.

The morphology of the cells was also observed using scanning electron microscopy (SEM). Cells were grown on plates, which were only partially covered with GO nanofilm. This enabled cells to be visualised on the GO surface and, above all, on the border of the GO surface and the surface of the plastic dish. The image of the cells after 7 days of culture allowed an assessment of their preferences for their placement on nfGO or outside of nfGO.

HS-5 cells were evenly located both on nfGO and outside nfGO as well as on the plastic/nfGO border. Cell settlement topography did not reflect the plastic/nfGO border line, although cells on nfGO had slightly longer protrusions and were more elongated (Fig. 6).

Liver cancer cells exhibit different culture behaviour, forming characteristic clusters that have been observed with HepG2. Cluster formation was observed both on the plastic surface of the culture vessel as well as on nfGO and at the plastic/nfGO border. Observation of the image of cells colonising on nfGO showed that the cells formed looser clusters with single cells more visible. The tendencies to create groups (clusters) were clearly smaller, and the adherence of individual cells to the GO substrate seemed larger (Fig. 7).

C3A cells, like HepG2, formed clusters, colonising both the GO surface and the plastic/nfGO border. In the nfGO group, slightly more single cells not bound into clusters were also observed (Fig. 8).

2.4. Influence of nfGO and CELE on cell proliferation

Cell proliferation was measured by using the test based on the measurement of BrdU incorporation during DNA synthesis (Fig. 9). The experimental factors did not affect the proliferation of non-tumour HS-5 cells. In contrast with HS-5 cells, nfGO, CELE, and to the greatest extent the combined factors (nfGO + CELE) reduced the proliferation of HepG2 cells. However, none of the experimental factors significantly influenced the proliferation of C3A cells.

2.4.1. Influence of nfGO and CELE on proliferation-associated gene expression at the mRNA level

In order to clarify the molecular basis of proliferation under the influence of the signal induced by the GO nanofilm and the addition of CELE, the mRNA expression of the *pcna*, *ki67*, and *mcm2* genes was studied (Fig. 10).

The cultivation of HS-5 cells on nfGO as well as on nfGO with CELE addition resulted in a decrease in *pcna* expression, an increase in *ki67* expression, and a tendency towards an increase in *mcm2* expression. However, the addition of CELE to the medium did not change the expression of the mitotic index markers.

HepG2 tumour cells showed a slightly different response to the factors tested. Surface modification by GO nanofilm was the reason for the increased expression of *ki67* and *mcm2*. This was in contrast to the CELE, which reduced the expression of all genes (*pcna*, *ki67* and *mcm2*). The effect of the GO surface was to reduce the CELE interaction on *pcna* expression. Moreover, the GO nanofilm eliminated the effects of CELE on *ki67*, and the combined use of these factors was the cause of overexpression of the *ki67* gene. A similar picture was observed in the case of *mcm2*, where the CELE effect was levelled by the surface treatment.

The influence of experimental factors on C3A cells was smaller. Some overexpression of the *ki67* and *mcm2* genes was observed under the influence of the GO nanofilm as well as the GO nanofilm together with the CELE (Table S3).

2.5. The cell-ECM and cell-cell connections

2.5.1. Integrin expression profile

The modification of the culture plate surface by using GO nanofilm increased the expression of *α1*, *α2*, *α3*, *α5*, *α6*, and *β4* and decreased the expression of *β1* integrins in non-cancer cells HS-5 (Fig. 11, Table S1). In turn, the addition of CELE elevated the expression of integrin *αV* and *β1* and reduced the *α2*, *α3*, and *β4* integrin mRNA level. The use of both factors (nfGO + CELE) caused overexpression of *α1, α3, α5*, and especially *α4, αV*, and *β1* in HS-5 cells.

Integrin expression in HepG2 cancer cells was completely different. A reduction in the *α3* and *α5* mRNA level was found, while an increase in *α1, α6, αV*, and *β4* was influenced by the use of GO surfaces. The opposite effect was observed under the influence of CELE for integrins *α1*, *α5*, *α6*, and *αV.* The use of both factors was clearly the cause of integrin overexpression *α2, α5, αV*, and *β4* in HepG2 cells (Table S2).

A different effect was observed in C3A tumour cells than in HepG2. First of all, no factor influenced downregulation of integrin expression. The surface of the nanofilm induced the integrin expression *α1*, *α2*, *α3*, *α6*, *αV*, *β1*, and *β4*, while CELE induced an increase in *α1*, *α2*, *α3*, *α6*, *αV*, and *β1* integrins (Table S3). Interestingly, the combined use of both factors (nfGO + CELE) resulted in a decrease in the expression of most integrins compared to their use separately.

Thus, mutual enhancement of the surface effect and addition of CELE to the culture medium was observed in non-tumour cells for *α4* and *αV* integrins and above all in HepG2 tumour cells for *α2*, *α5*, *αV*, and *β4* integrins.

2.5.2. Focal adhesion kinase, cadherins and β-catenin

Gene expression for key proteins involved in the integration of mechano- and chemo-signalling between ECM-cell and cell-cell, as *fak*, *e-cadherin*, *n-cadherin*, and *β-catenin* are presented in Fig. 12. By analysing gene expression in HS-5 cells, it was found that the surface modification by GO only significantly increased the expression of *n-cadherin*, while the CELE did not affect the results. The combined use of nfGO + CELE resulted in significant overexpression of all adhesion markers (Table S1).

In the HepG2 liver cancer line, the use of GO nanofilm resulted in a significant increase in the expression of genes responsible for cell-ECM adhesion (*fak*) as well as cell-cell adhesion (*cadherins*). Moreover, nfGO decreased the expression of *β-catenin*. Unlike other genes, the expression of *β-catenin* was also downregulated by CELE. The use of both factors (nfGO + CELE) clearly increased the expression of *fak*, *e-cadherin*, and *n-cadherin* and reduced the expression of *β-catenin* (Table S2).

C3A cells cultured on nfGO showed higher expression of *fak* compared to the control group. Furthermore, we found that the CELE supplementation increased *n-cadherin* expression. Nanofilm GO with additive CELE increased *n-cadherin* and *β-catenin* expression of C3A cells (Table S3).

2.6. Effect on cell cycle

To investigate whether the mechanical signal from nfGO and a molecular signal from a CELE influence cell cycle, flow cytometric analysis was performed (Fig. 13). HS-5 cells cultured on GO nanofilm as well as cultured with additives of CELE but also treated nfGO + CELE for 7 days showed a decrease in the population of cells in S phase with a concomitant slight increase in the G0/G1 phase. Simultaneously, a reduction in the cell population in the G2/M phase was observed under the influence of CELE and nfGO + CELE.

In HepG2 cells, in contrast to non-tumour cells, a decrease in the G0/G1 phase population under the influence of nfGO + CELE slightly increased the S population, and an increase in the G2/M phase population was observed.

Observation of C3A cells showed no effect of the GO surface on the cell cycle, although the CELE and nfGO + CELE slightly increased the population of cells in the S phase and decreased the population of cells in the G2/M phase.

3. Discussion

Mutual interaction, signalling and cooperation between the ECM and the cell, and, moreover, the principle of feedback in these relationships are key factors determining the fate of the cell [5, 25]. In the present research, we wanted to clarify whether a change in the basic physicochemical parameters of the surface

(mimic ECM) will change the behaviour of the cell, and especially whether it will reduce its carcinogenic potential. However, based on previous studies, we have shown that modification of the surface ECM changes the cell's demand for functional molecules so that the surface effect also depends to a large extent on the chemical compounds available to the cell, mainly proteins [19, 26]. Therefore, an attempt was made to force the cell to change its behaviour (weakening its invasiveness) by physicochemical modification of its niche together with supplying its environment with a wide spectrum of potentially useful proteins. For the first time, it has been shown that the use of mechanical stimulation with the addition of a protein cocktail can activate transmembrane signalling mechanisms and consequently decrease the proliferation of HepG2 liver cancer cells and reduce their carcinogenic potential.

In the present study, the surface of the culture plate was modified by a thin layer of GO which formed a nanofilm that could act on receptors located on the cell membrane but was not internalised by cells [27]. The newly created surface (nfGO) was a source of mechanical and chemical signal modification. The reduction of stiffness (2.3 GPa) and the increase in roughness by the nfGO, compared to clean polystyrene (3-3.5 GPa) [15, 17], resembles the differences between normal and fibrotic tissue [28, 29]. Moreover, the negative charge that characterised GO also favourably changed the surface that imitated the negative charge of proteoglycans and hyaluronic acid, as opposed to collagen [30, 31]. The beneficial change in GO surface properties also concerned increasing their hydrophilicity by the presence of numerous oxygen groups, such as hydroxyl (-OH), carboxylic (-COOH), and epoxide (-O-) [23].

The second factor, the source of the cocktail of various proteins, was chicken liver embryo extract. The unpredictable demand of cells for signalling growth-structural factors under the influence of the modified surface (mimic ECM) determined the choice of CELE. Namely, a unique phenomenon of embryo growth and development has been used, consisting, inter alia, in creating a perfect, dynamic niche for extremely fast proliferating cells [12, 21, 32]. Most of the proteins from CELE were part of the perfect ECM/niche. CELE provided two types of laminins (LAMA1 and LAMC1), whose level is reduced in HCC [5], and also only two types of collagen (COL12A1 and COL5A1) that are detected in healthy tissue but not in cancer tissue [33]. Other important proteins include fibronectin (FN1) and vitronectin (VTN), which are responsible for the regenerative process [6, 34]. The extract also contained functional proteins responsible for ECM modification, tight cellular connections, migration, EMT, and asymmetric cell division in embryogenesis and proliferation. However, the behaviour of the CELE should be considered as a dynamically migrating and changing structure and above all one that potentially interacts in two directions. The first is direct contact and signalling to the cell, while the second is depositing the GO nanofilm and building the mimic ECM/niche structure [15, 20]. The high roughness of the GO surface enriched with π electrons can promote cell adhesion and adsorption of ECM proteins through noncovalent π-π stacking interactions [35, 36] and form the so-called protein corona [37, 38, 39].

The first line of contact between the cell and the ECM are integrins, which in response to signals from outside transmit information to the cell and are the source of the signalling cascade covering most of its functions [5, 40, 41]. Integrins, heterodimeric receptors, belong to the family of adhesive proteins and contain 18 alpha subunits and 9 beta subunits occurring in 24 alpha-beta combinations [42]. However, a

high level of expression of one subunit may be sufficient to alter the expression of the entire heterodimer [43]. Nine key integrin subunits were identified in the conducted studies. Interestingly, the expression of examined integrins under the influence of both the surface and the CELE was definitely different in HepG2, C3A, and non-cancer HS-5 cells, which demonstrated the different sensitivity of various types of cells or/and tumours to mechanical and chemical signalling derived from the cell microenvironment. Thus, the mechanical characteristics of the substratum can be expressed due to the dynamics of integrin clusters in a cell-specific manner [44]. What's more, it confirms the thesis of the need for targeted therapy and the risk of obtaining a negative effect in mismatched therapy. Additionally, C3A cells cause a higher resistance to treatment than the HepG2 cell line [16]. C3A cells produce more albumin and alpha-fetoprotein than HepG2 cells and can grow in the glucose-deficient medium. Albumins and alpha-fetoprotein from C3A can adsorb onto nanomaterials, form protein corona, change the interaction nfGO-cells, and mitigate the effect of nfGO [45, 46].

Studies on integrin expression still do not allow for an unambiguous arrangement of their role and significance depending on the type of cells, type of cancer and phenotype of cancer cells, stage of cancer, and metastasis. Nevertheless, numerous studies have allowed for the creation of a map of plausible integrin heterodimers as therapeutic cancer targets [42]. Based on the analysis of the expression of selected integrins in liver tumours compared to healthy tissue, αV and β1 subunits can be indicated as the most frequently recurring in typed heterodimers [40, 43]. In our studies, the expression of *β1* integrins did not change under the influence of the factors used in HepG2 cells, in contrast to C3A cells. This confirms the diverse response of different types of tumours and above all may suggest the procancerogenic activity of both nfGO and CELE for the C3A tumour line. Analysis of *αV* integrin expression also confirms the adverse effects of the CELE and nfGO in C3A cells. However, in HepG2 cells, the expression of integrin *αV* was lower under the influence of CELE, although higher under the influence of surface modification with GO nanofilm. Integrin αV is upregulated in many tumour cells, making it a promising therapeutic target. Most integrins, including αV, can bind various ligands, *e.g.*, fibronectin and vitronectin [42]. Despite the presence of these ligands in the extract, there was no increase in expression of the *αV* subunit, which is considered to be a marker of liver fibrosis. In addition, the extract reduced expression of the *α6* subunit, which is involved in treatment resistance, spheroid and exosome formation, and metastasis [34, 47]. An inhibitor of αV integrin is a new drug for the treatment of glioblastomas that is being verified in a phase III clinical trial [43]. However, this therapeutic method of blocking integrin antibodies is not an excellent solution and is not always effective. The reason for the ineffectiveness of such a therapy may be that integrin overexpression may be a survival signal and result from feedback (ECM - cell) in which the cell does not adhere to a degraded niche, which in turn promotes metastasis [48]. Thus, the desperate attempt of the cell to contact the ECM/niche and consequently the increase of integrin expression may be greater the more its environment is degraded. Paradoxically, despite being a kind of "striving for normality", it is proportional to the carcinogenicity and metastasis potential. Moreover, most studies do not take into account the physicochemical state of the extracellular matrix, which is the largest regulator of integrin expression and activity, especially when faced with a very large number of ligands present in the ECM and cell surface adhesion proteins that bind integrins. The presence or absence of specific ligands in the

ECM appears to be crucial for integrin expression and status. Culturing HepG2 cells on nfGO reduced the expression of the laminin binding *α3* integrin and fibronectin binding *α5* subunits in HepG2 cancer cells [41]. Laminin and fibronectin are involved in the formation of dynamic cell binding to ECM. Furthermore, they mediate cell binding to collagen [12]. The α5β1 integrin is the most important fibronectin receptor that binds to RGD-containing peptides. It can be assumed that the GO nanofilm has become a structure that imitates laminin and fibronectin, becoming a surface that promotes HepG2 cell adhesion [15, 49]. Although it seems more likely that the protein corona, made up of proteins available in the culture medium, exposed ligand-like structures on the surface. However, by analysing the expression of α *5*, overexpression of this gene was observed when CELE was added to the culture medium. This expected effect was probably the result of the increased availability of ligands (fibronectin) in the culture medium, whose source was CELE, and activation of their binding to alpha 5 integrin, however, independent of the surface. Interestingly, surface modification and simultaneous addition of CELE increased the expression of the integrin *α5* subunit, which can be explained by the increased availability of ligands through binding them to the GO nanofilm. The GO nanofilm roughness was greater than the culture plastic plate, but also proteins' noncovalent π-π stacking interactions [35] could increase the amount of bottom-related proteins. Furthermore, this interaction could be preferentially directed to the RGD-mimicking GO motif due to tryptophan, which also has π-π interactions due to the aromatic ring [35, 50]. Moreover, the use of both factors enhanced expression of the *α5* subunit to the greatest extent. This integrin is involved in cell strong adhesion, and thus we paid attention to the proteins involved in cell-ECM and cell-cell adhesion mechanisms.

Mechanotransduction resulting from integrin clustering dynamics, depending on the rigidity of the substrate, is associated with FAK phosphorylation [44]. The expression of *fak* increased in HS-5 and HepG2 cultivated on GO with CELE supplementation. GO may reduce [41, 51] or enhance *fak* expression [52], which may depend on the presence of ligands, and consequently in our research, CELE was added to prevent this. Liver cells are anchor-dependent cells in which the level of *fak* increases in suspension culture [53, 54, 55]. The tested cells adhered tightly to the surface, so overexpression of *fak* resulted from increased *via* integrin signalling, conditioned by strong cell adhesion to nfGO + CELE, and it could be a signal of cell survival in the proadhesive but antiproliferative niche [56].

The cadherin-catenin complex carries the mechanotransduction signal between the cytoplasm of neighbouring cells [57]. High expression of E-cadherin is a characteristic feature of epithelial cells; it inhibits translocation of β-catenin into the nucleus and promotes better prognosis in cancer therapy [58]. Expression of adhesive protein genes such as *e-cadherin* and *n-cadherin* was higher under the influence of GO nanofilm and nfGO + CELE, especially in HepG2 cells, but most important was a reduction in *β-catenin* expression in these cells [11, 54, 59]. Our results, like Mu *et al*., showed that cells increase the expression of E-cadherin on nfGO, moreover, in view of the fact that the weakening of tight connections (E-cadherin expression) and an increase in flexible cell-cell contacts (N-cadherin expression) is characteristic of HCC [21]. Thus, the increase in expression of two types of intercellular junctions suggests that the experimental factors used (nfGO and CELE) did not increase the invasion of HepG2

cells [21, 59, 60]. These results are also confirmed by the observation of cell morphology, which reflects the cell-ECM and cell-cell relationship and also indicates material biocompatibility [32, 61, 62, 63].

First of all, tendencies to form smaller cell clusters and a larger number of single cells strongly associated with the GO surface were observed in both HepG2 and C3A groups. This confirms the biocompatibility of the GO plane [17] and also indicates one- and several-cell migration instead of collective migration, which is characteristic of abnormal ECM [64]. Furthermore, the roughness and elasticity of GO as a mimic ECM could advantageously imitate the natural ECM mosaic, and it was preferentially selected by all cells [15]. The effect of CELE was slightly different for HS-5 cells and liver cancer cells. This may be due to the fact that it contained more ligands and other factors needed by the liver cell rather than the connective tissue cell. Our research and that of other authors may indicate that extracts from chicken embryo [21], zebrafish [65], and amphibian oocyte [66] are excellent cocktails of factors preventing metastatic phenotype.

External mechanical-chemical stimuli, received through integrin-dependent mechanisms transmitted to the cell, create a cascade of events that determine the fate and purpose of the cell. Analysing the cell cycle, it was observed that the population in G0/G1 phase decreased only in the case of HepG2 cells. Furthermore, *mcm2* and *pcna* gene analysis confirmed a decrease in cell population in G1 and S phases, respectively. Our research and Wang *et al.* showed that overexpression of the *α5* subunit inhibits the proliferation and invasiveness of cancer cells [67]. The reason for this phenomenon could be the mechanism we observed *via* integrins and adhesion components passed on to the cell. The results obtained indicate activating Mek/Erk, PI3K/Akt, and the small GTPase Rac pathways which are involved in the synthesis of cyclins (D1 and E) and the transition of cells from the G1 phase to the S phase by integrin signalling and physical interaction of integrins with growth factors and growth factor receptors (EGFR and VEGFR). Therefore, proper cell adhesion overcame the first proliferation checkpoint [68]. In most human cancers, the G0/G1 checkpoint does not completely stop the cell cycle as opposed to G2/M [69]. In the present work, the use of two factors (nfGO + CELE) increased the population of HepG2 and C3A cells in the G2/M phase, thus preventing cells with damaged DNA from entering the M phase and allowing damage repair [16]. Ultimately, the total population of HepG2 cells in the active phase of the cell cycle was increased, in particular in G2/M phase, which confirms the increase in the *ki67* gene expression. Moreover, many extract proteins (including nitrilase 2 (NIT2), DNA-binding protein 43 (TARDBP) and dynein light chain) adsorbed on nfGO or available in the medium may have been involved in arresting the cell cycle in the G2/M phase [65, 70, 71]. Our results and Jabaily *et al.* confirm that liver extract was a universal source of missing proteins, and in the future, it may modulate the proliferation of various cell lines including bone marrow and muscle cells [32]. The final and fundamental evidence of the loss of HepG2 cell invasiveness is a reduction of proliferation in the BrdU test of more than 40% compared to the control, which was not observed in non-cancerous cells.

All of these data indicate that graphene oxide and a cocktail of proteins that formed the dynamically changing proteome of the cell environment, migrating in the culture medium to the GO plane and the cell and therefore available multilevel (as a source of ligands and other proteins and as a modulator of the

chemical characteristics of the GO surface), may have therapeutic effects on HepG2 liver cancer. ECM-therapy may have the effect of supporting traditional treatment, especially since degraded ECM characteristic for tumours becomes a pro-tumour factor and in any case hinders treatment.

Conclusions

In the present study, we indicated the possibility of using the so-called ECM-therapy as an option to support the treatment of some cases of liver cancer. For the first time, it has been documented that for the HepG2 cancer cell line, the use of mimic ECM in the form of a graphene oxide surface enriched with a natural protein cocktail, being the source of ligands for integrins and a wide range of other missing proteins, is the source of a mechano-chemo transduction signal. This signal, via integrin expression, adhesion, morphology change, and cell cycle arrest in the G2/M phase, reduces the proliferation of tumour cells. The research is preliminary and requires further precise experiments.

Methods

3.1. *Characterisation of GO nanoparticles and GO nanofilms*

3.1.1. Characterisation of GO nanoparticles

GO flakes, as a water dispersion at a concentration of 4 mg/mL, were purchased from NANOPOZ (Poznan, Poland) and produced by the modified Hummers method. This nanomaterial, after dispersion into ultrapure Milli-Q water to prepare 50 mg/L solutions, was sonicated for 15 minutes in an ultrasonic bath (Bandelin Electronic, Berlin, Germany) to avoid agglomeration. The shape and size of the GO flakes were characterized using transmission electron microscopy (TEM: JEM-1220 JEOL, Tokyo, Japan). TEM was connected to a camera (SIS Morada 11 megapixels) and operated by ITEM Olympus Soft Imaging Platform. Six pictures were taken of two independent samples. Zeta potential was measured in triplicate with a Nano-ZS90 Zetasizer (Malvern Instruments, Malvern, UK) operated by Zetasizer software 7.13.

The Fourier transform infrared spectra of GO were acquired using a Perkin Elmer System 2000 instrument (MA, USA) operated by Pegrams software in the range of 400–4000 cm^{-1}. Solid-state samples were milled with potassium bromide (KBr) crystals in an approximate ratio of 1:300 mg. The solid mixture was milled in a laboratory mill (Specac) to obtain a fine powder. Then, 8 tons of pressure was applied for 2 min to prepare transparent thin pellets. A total of 25 scans were conducted for every sample. The infrared absorption of water vapour and carbon dioxide was mostly eliminated. Spectra were processed with baseline correction and Fourier smoothing, with 90% smoothing, to remove undesired noise. Spectra are presented as transmission (dependent variable) against wavenumber (independent variable).

3.1.2. Preparation and characterisation of GO nanofilms

A GO aqueous solution (1000 mg/L) was sonicated for 30 min before preparing the nanofilm. GO was used to form nanofilms by applying the solution to the bottom of ordinary polystyrene plates (353046,

Falcon, Tewksbury, MA, USA) [72]. A GO solution was dried at room temperature in a laminar chamber for day. A 1 cm^2 polystyrene surface was covered with 105 µg of carbon solution. As a result of self-assembly, the resultant surface was a stable, thin surface nanofilm that adhered perfectly to the bottom of the plastic wells. Thus, GO coating was deposited on polystyrene plates by solvent evaporation from graphene nanoflake solutions. However, the nanofilm could be damaged when taking it out.

The AFM method (Nanosurf, Liestal, Switzerland) was used to characterise the morphology of the plastic plate and GO coated plate including average roughness and maximum height of the roughness. Six pictures were taken of two independent samples.

The water contact surface on an uncoated and GO coated surface was measured by the sessile drop technique, *i.e.*, a 20 µl drop of water was placed on the investigated surface and a picture was taken. Five measurements of the contact surface were detected to characterise the GO film wettability during liquid spreading and dewetting using a stereomicroscope (SZX10, CellD software version 3.1; Olympus Corporation, Japan). Water area (mm^2) was calculated using ImageJ® 1.48v (National Institutes of Health, Bethesda, MD, USA).

To evaluate the preferences of cell placement on and outside the nanofilm, the GO colloidal solution partially coated the culture plate. After the GO nanofilm was dried, we were able to observe cell migration and the affinity of cells to the nanofilms using TEM.

3.2. *Preparation and characterisation of extract (CELE)*

3.2.1. Preparation of CELE and bicinchoninic acid protein assay (BCA)

Livers from 10-day chicken embryos were removed and used for protein isolation. Whole-liver protein extracts were prepared with a TissueLyser LT instrument (Qiagen, Hilden, Germany) using 8 g of tissue and 20 ml of MilliQ-water. The homogenate was centrifuged at 3000 rpm for 10 min. The precipitate was removed, and the supernatant was transferred to new tubes. The total protein content was determined in six repetitions using a BCA Protein Assay Kit according to the manufacturer's recommendations (Sigma-Aldrich, St. Louis, MO, USA). The extract was added at a volume ratio of 1 ml of extract per 100 ml of Dulbecco's Modified Eagle's Medium (DMEM) to obtain a 1% extract in DMEM.

3.2.2. Mass Spectrometry

Protein extract (150 µl, 24.6 mg/ml) was concentrated using Vivacon 500, 10 000 MWCO hydrosart filters and washed twice. Proteins were reduced by the addition of 50 µl of washing buffer (8 M urea in 100 mM NH_4HCO_3 aqueous solution) with 20 mM tris(2-carboxyethyl) phosphine and incubated for 30 min. After centrifugation, proteins were alkylated with 50 µl of 20 mM indole-3-acetic acid in washing buffer and then spun. Digestion was performed with the protease mix LysC/Tryp (V507A, Promega, Madison, WI, USA). First, 40 µl of a solution was added to the filter and incubated for 3 h at 37 °C, and then, 400 µl of

NH_4HCO_3 was added, and samples were incubated overnight at 37 °C. After centrifugation, the solution was acidified with a final concentration of 0.4% trifluoroacetic acid (TFA) and speed-vacuumed to dryness. The peptide mixture was fractionated using a high pH protocol on an Oasis HLB 10 mg cartridge (Waters 186000383). Cartridges were activated by washing with methanol and equilibrated with 25 mM ammonium formate, pH 10. The protein pellet was resuspended in 400 µl of 25 ammonium formate (pH 10) and loaded on a cartridge. The elution was carried out with an increasing gradient of acetonitrile in loading buffer and with pure methanol (last elution). All fractions were dried, and pellets were resuspended in 60 µl of 0.1% TFA with 2% MeCN. MS analysis was performed *via* LC-MS in the Laboratory of Mass Spectrometry (IBB PAS, Warsaw) using a nanoAcquity UPLC system (Waters) coupled to an LTQ-Orbitrap Q Exactive mass spectrometer (Thermo Fisher Scientific, Waltham, MA, USA). The mass spectrometer was operated in the data-dependent MS2 mode, and data were acquired in the m/z range of 200–2000. Peptides were separated by a 180 min linear gradient of 95% solution A (0.1% formic acid in water) to 45% solution B (acetonitrile and 0.1% formic acid). The measurement of each sample was preceded by three washing runs to avoid cross-contamination. Data were analysed with the Max-Quant 1.6.3.4 platform [73, 74]. The *Gallus gallus* reference proteome database from UniProt was used.

3.3. *Cell cultures and treatments*

The liver cancer cell lines HepG2 (HB-8065) and C3A (CRL-10741) and the non-cancer bone marrow stromal cell line HS-5 (CRL-11882) were obtained from ATCC (Manassas, VA, USA). Cell cultures were maintained at 37 °C under 5% CO_2 in DMEM, Low Glucose (Gibco, Thermo Fisher Scientific) supplemented with 10% foetal bovine serum (FBS, Thermo Fisher Scientific), penicillin (100 U/mL), and streptomycin (100 mg/mL, Thermo Fisher Scientific). Cells were seeded on 6-well plates (1.5×10^5 cells in each well), and the cultures were maintained for 48 h and 7 days.

All experiments were conducted according to the following scheme: (1) no treatment group - control; (2) group using the nfGO; (3) group with the addition of CELE in an amount of 1% of the culture medium - CELE; (4) group using the nfGO with the addition of CELE in an amount of 1% of the culture medium - nfGO + CELE. CELE components were added as serum-like supplements to medium. The medium containing CELE was incubated on nfGO at 22 °C for 5 min. Finally, the cells were added onto the CELE-loaded nfGO.

3.4. *BrdU assay*

Cell proliferation was studied using a bromodeoxyuridine (BrdU) incorporation assay (BrdU colorimetric) (Roche Applied Science, Indianapolis, IN, USA). HS-5, HepG2, and C3A cells were seeded in the 96-well microplates according to the scheme described in the ”Cell cultures and treatments” section at a concentration 7×10^3 cells/well. All of the treatment groups were examined in six repetitions. Cells were cultivated for 24 h, and then 20 µl of 100 µM BrdU solution in DMEM was added to each well of the cultured cells. The cells were labelled with BrdU for 24 h. All further steps were carried out according to

the manufacturer's instructions. Cell proliferation was analysed using a Tecan Infinite 200 microplate reader at 370 nm with a reference wavelength of 492 nm.

3.5. *Microscopy*

3.5.1. Light microscopy

To assess cell morphology, an inverted light microscope (Leica, TL-LED, Wetzlar, Germany) was used. The instrument was connected to a digital camera (Leica MC190 HD) and operated with LAS V4.10 software (Leica). The cells were stained using haematoxylin-eosin after 48 h of incubation. Six pictures were taken of two independent samples.

3.5.2. Scanning electron microscopy

Microstructures of cell morphology were evaluated using SEM. HS-5, HepG2 and C3A cells were seeded on 6-well plates uncoated and coated with nfGO. After 7 days of exposure, the cells were rinsed in phosphate-buffered saline (PBS, pH 7.2) and then fixed in 2.5% glutaraldehyde (G5882, Sigma-Aldrich) for 20 min. Cells were incubated in osmium tetroxide (OsO_4) and then in freshly made 1% carbohydrazide and fixed again in OsO_4 for 30 min. After thorough rinsing, the plates were cut to fit the critical point dryer (Polaron CPD 7501, Quorum Technologies, Laughton, UK). Cells were dehydrated through a hexylene glycol series (Sigma-Aldrich). Samples were placed on aluminium SEM stubs. Six pictures were taken of two independent samples.

3.6. *Flow cytometry*

The cell cycle was evaluated using flow cytometry (FACSCalibur, Becton Dickinson, Franklin Lakes, NJ, USA). Cell cycle analysis, based on DNA content, was performed according to the UC San Diego Health Sciences protocol [75] using CellQuest Pro software. Cells were cultured in 6-well plates for one week as described in the section "Cell cultures and treatments". Cells were detached with trypsin, which was neutralized with fresh DMEM. After centrifugation, cell pellets were washed, resuspended in PBS (1 ml), fixed with 9 volumes of 70% ethanol at 4 °C for 24 hours. For propidium iodide (PI, 500 µg/mL) staining, after centrifugation, each sample of cells was resuspended in 500 µl of staining solution. The staining solution contained RNAse A (2 µl, Thermo Fisher Scientific), PI (20 µl, Thermo Fisher Scientific), Tween 20 (0.5 µl), and PBS (477.5 µl). After incubation for 30 min, the cells were analysed by flow cytometry by measuring the fluorescence emission at 530 nm and 575 nm (or equivalent) using excitation at 488 nm. Each measurement was repeated three times.

3.7. *Gene expression*

3.7.1. RNA isolation

Cell cultures were maintained according to the previously described scheme. After 7 days of incubation, cells in 6-well plates were detached with trypsin and collected by centrifugation. All steps of RNA isolation were performed according to the protocol from the manufacturer Macherey-Nagel (No. 740955.250,

Düren, Germany). The RNA concentration in each sample after isolation was determined using a NanoDrop 2000 spectrophotometer (Thermo Fisher Scientific). RNA was stored at -80 °C.

3.7.2. DNA synthesis

The RNA level in all samples was equalized, and 10 µL of RNA mixture in water was used for cDNA synthesis using a High-Capacity cDNA Reverse Transcription Kit (No. 4368814, Applied Biosystems, Foster City, CA, USA). The procedure was performed according to the manufacturer's protocol with the following cycle conditions: 10 min at 25 °C, 120 min at 37 °C and store at 4 °C. cDNA synthesis was performed using a 2720 Thermal Cycler (Thermo Fisher Scientific). ssDNA concentration was measured with the NanoDrop 2000 (Thermo Fisher Scientific), and 300 µl of 20 ng/µL ssDNA was prepared. ssDNA samples were kept at -20 °C.

3.7.3. RT-PCR

Gene expression at the mRNA level was measured using the ΔΔCT relative quantification real-time PCR method. The reaction mixture was prepared using Power SYBR™ Green PCR Master Mix (Thermo Fisher Scientific), 10 µM forward primers, 10 µM reverse primers, and RNase/DNase-free water at a ratio of 10:1:1:1.3. Then, 5 µl of 100 ng of ssDNA was added to 10 µl of the reaction mixture. The primers used for real-time PCR are presented in Table 2. *Glyceraldehyde-3-phosphate dehydrogenase* (*gapdh)* was used as the reference house-keeping gene. The study was performed using a StepOnePlus™ Real-Time PCR System (Thermo Fisher Scientific) with the following settings: 95 °C for 10 min, followed by 40 cycles of 95 °C for 15 s and 60 °C for 60 s. StepOneTM Software 2.2.2 was used to asses gene expression. All reactions were performed in triplicate, and the experiment was run two independent times. The ΔCT value was calculated from the formula CT gene – CT *GAPDH* and used to investigate statistical significance. The -ΔΔCT value is expressed as the relative gene expression (ΔCT control – ΔCT treated group).

Table 2
Primers used to evaluate the expression of genes involved in proliferation and cell adhesion

Gene	Sequence of primer 5'->3'	Amplicon size (bp)	GenBank accession number	Reference
pcna	F: CCATCCTCAAGAAGGTGTTGG	710	NM_182649.2	PrimerBlast
	R: GTGTCCCATATCCGCAATTTTAT			
ki67	F: CCACACTGTGTCGTCGTTTG	123	NM_001145966.2	[76]
	R: CCGTGCGCTTATCCATTCA			
mcm2	F: GTGGATAAGGCTCGTCAGAT	87	NM_004526.4	[76]
	R: GTCGTGGCTGAACTTGTT			
α1	F: GGTTCCTACTTTGGCAGTATT	149	NM_181501.2	[77]
	R: AACCTTGTCTGATTGAGAGCA			
α2	F: GGAACGGGACTTTCGCAT	154	NM_002203.4	[77]
	R: GGTACTTCGGCTTTCTCATCA			
α3	F: AAGGGACCTTCAGGTGCA	129	NM_002204.4	[77]
	R: TGTAGCCGGTGATTTACCAT			
α4	F: GCTTCTCAGATCTGCTCGTG	131	NM_000885.6	[77]
	R: GTCACTTCCAACGAGGTTTG			
α5	F: TGCAGTGTGAGGCTGTGTACA	88	NM_002205.5	[77]
	R: GTGGCCACCTGACGCTCT			
α6	F: TTGAATATACTGCTAACCCCG	113	NM_000210.4	[77]
	R: TCGAAACTGAACTCTTGAGGATAG			
αV	F: AATCTTCCAATTGAGGATATCAC	140	NM_001145000.3	[77]
	R: AAAACAGCCAGTAGCAACAAT			
β1	F: GAAGGGTTGCCCTCCAGA	107	NM_002211.4	[77]
	R: GCTTGAGCTTCTCTGCTGTT			
β4	F: AGACGAGATGTTCAGGGACC	115	NM_001321123.2	[77]
	R: GGTCTCCTCTGTGATTTGGAA			
fak	F: CCCACCAGAGGAGTATGTCC	150	XM_017013688.2	[78]
	R: CCCAGGTCAGAGTTCAATAG			

Gene	Sequence of primer 5'->3'	Amplicon size (bp)	GenBank accession number	Reference
e-cadherin	F: ACAACGCCCCCATACCAGA R: CACTCGCCCCGTGTGTTAGT	138	NM_001317185.2	PrimerBlast
n-cadherin	F: ACAGATGTGGACAGGATTGTGGGT R: TATCCCGGCGTTTCATCCATACCA	124	NM_001308176.2	PrimerBlast
β-catenin	F: CCTATGCAGGGGTGGTCAAC R: CGACCTGGAAAACGCCATCA	95	NM_001012329.2	PrimerBlast
gapdh	F: GAGAAGGCTGGGGCTCATTTG R: CATGGTTCACACCCATG	97	NM_002046	PrimerBlast

3.8. *Statistical analysis*

The data were analysed *via* one-way analysis of variance – ANOVA (for analysis of more than two research groups) or an unpaired t-test using GraphPad Prism software version 8.1.2 (GraphPad Software Inc., La Jolla, CA, USA). The differences between the groups determined using ANOVA were assessed with Bonferroni's multiple comparisons test. Differences with a p-value ≤ 0.05 were defined as statistically significant: one asterisk (*), p-value < 0.05; two asterisks (**), p-value < 0.01; three asterisks (***), p-value < 0.001.

Abbreviations

AFM: Atomic force microscopy

ANOVA: Analysis of variance

ATCC: American type culture collection

BCA: Bicinchoninic acid protein assay

BrdU: Bromodeoxyuridine

CELE: Chicken embryo liver extract

Col12A1: Collagen alpha-1(XII) chain

Col14A: Collagen alpha(XIV) chain

Col16A: Collagen alpha(XVI) chain

Col5A1: Collagen alpha-1(V) chain

DMEM: Dulbecco's Modified Eagle's Medium

ECM: Extracellular matrix

EGFR: Epidermal growth factor receptor

EMT: Epithelial-mesenchymal transition

FAK: Focal adhesion kinase

FBS: Foetal bovine serum

FN1: Fibronectin

FTIR: Fourier transform infrared

GAPDH: Glyceraldehyde-3-phosphate dehydrogenase

H&E: Hematoxylin and eosin

HBV: Hepatitis b virus

HCC: Hepatocellular carcinoma

HCV: Hepatitis c virus

LAMA1: Laminin subunit alpha-1

LAMC1: Laminin subunit gamma-1

MCM2: minichromosome maintenance protein complex 2

nfGO: Graphene oxide nanofilm

NIT2: Nitrilase 2

PBS: Phosphate-buffered saline

PCNA: Proliferating cell nuclear antigen

PI: Propidium iodide

SEM: Scanning electron microscopy

TARDBP: DNA-binding protein 43

TEM: Transmission electron microscopy

TFA: Trifluoroacetic acid

VEGFR: Vascular endothelial growth factor

VTN: Vitronectin

Declarations

Ethics approval and consent to participate

Not applicable

Consent for publication

Not applicable

Availability of data and materials

The datasets used and/or analysed during the current study are available from the corresponding author on reasonable request.

Competing interests

The authors declare that they have no competing interests.

Funding

This research was carried out in the framework of project National Science Centre Poland nr. 2019/33/N/NZ7/01392.

Author’s contributions

Conceptualisation, M.S., E.S. and M.K.; methodology, M.S., S.J. and M.K.; software, E.S.; validation, M.S., E.S. and M.K.; formal analysis, M.S. and A.C.; investigation, M.S., B.S., J.S., P.K. and J.B.; resources, E.S., M.S, M.K. and W.B.; data curation, M.S. and K.D.; writing—original draft preparation, M.S.; writing—review and editing, E.S., W.B. and A.C.; visualisation, M.S.; supervision, E.S.; project administration, A.C.; funding acquisition, M.S. and W.B.

All authors read and approved the final manuscript.

Acknowledgements

This report is a part of Malwina Sosnowska's PhD thesis.

References

1. Baglieri J, Brenner DA, Kisseleva T. The role of fibrosis and liver-associated fibroblasts in the pathogenesis of hepatocellular carcinoma. Int J Mol Sci. 2019;20:1723. https://doi.org/10.3390/ijms20071723.
2. Hernandez–Gea V, Toffanin S, Friedman SL, Llovet JM. Role of the microenvironment in the pathogenesis and treatment of hepatocellular carcinoma. Gastroenterology. 2013;144:512-527. https://doi.org/10.1053/j.gastro.2013.01.002.
3. Lu P, Weaver VM, Werb Z. The extracellular matrix: A dynamic niche in cancer progression. J Cell Biol. 2012;196:395–406. https://doi.org/10.1083/jcb.201102147.
4. Iredale JP, Thompson A, Henderson NC. Extracellular matrix degradation in liver fibrosis: biochemistry and regulation. Bba-Mol Basis Dis. 2013;1832:876-883. https://doi.org/10.1016/j.bbadis.2012.11.002.
5. Carloni V, Luong TV, Rombouts K. Hepatic stellate cells and extracellular matrix in hepatocellular carcinoma: more complicated than ever. Liver Int. 2014;34:834-843. https://doi.org/10.1111/liv.12465.
6. Klaas M, Kangur T, Viil J, Mäemets-Allas K, Minajeva A, Vadi K, *et al.* The alterations in the extracellular matrix composition guide the repair of damaged liver tissue. Sci Rep-Uk. 2016;6:27398. https://doi.org/10.1038/srep27398.
7. Saneyasu T, Akhtar R, Sakai T. Molecular cues guiding matrix stiffness in liver fibrosis. Biomed Res Int. 2016;2016:2646212. https://doi.org/10.1155/2016/2646212.
8. Humphrey JD, Dufresne ER, Schwartz MA. Mechanotransduction and extracellular matrix homeostasis. Nat Rev Mol Cell Bio. 2014;15:802-812. https://doi.org/10.1038/nrm3896.
9. DeBerardinis RJ, Chandel NS. Fundamentals of cancer metabolism. Sci Adv. 2016;2:e1600200. https://doi.org/10.1038/nrc2981.
10. Han T, Kang D, Ji D, Wang X, Zhan W, Fu M, *et al.* How does cancer cell metabolism affect tumor migration and invasion? Cell Adhes Migr. 2013;7:395-403. https://doi.org/10.4161/cam.26345.
11. Kim E, Lisby A, Ma C, Lo N, Ehmer U, Hayer KE, *et al.* Promotion of growth factor signaling as a critical function of β-catenin during HCC progression. Nat Commun. 2019;10:1909. https://doi.org/10.1038/s41467-019-09780-z.
12. Walker C, Mojares E, del Río Hernández A. Role of extracellular matrix in development and cancer progression. Int J Mol Sci. 2018;19:3028. https://doi.org/10.3390/ijms19103028.

13. Baiocchini A, Montaldo C, Conigliaro A, Grimaldi A, Correani V, Mura F, *et al.* Extracellular matrix molecular remodeling in human liver fibrosis evolution. PloS One. 2016;11:e0151736. https://doi.org/10.1371/journal.pone.0151736.
14. Kutwin M, Sawosz E, Jaworski S, Wierzbicki M, Strojny B, Grodzik M, *et al.* Nanocomplexes of graphene oxide and platinum nanoparticles against colorectal cancer Colo205, HT-29, HTC-116, SW480, liver cancer HepG2, human breast cancer MCF-7, and adenocarcinoma LNCaP and human cervical Hela B cell lines. Materials. 2019;12:909. https://doi.org/10.3390/ma12060909.
15. Chaudhuri PK, Loh KP, Lim CT. Selective accelerated proliferation of malignant breast cancer cells on planar graphene oxide films. Acs Nano. 2016;10:3424-3434. https://doi.org/10.1021/acsnano.5b07409.
16. Sosnowska M, Kutwin M, Jaworski S, Strojny B, Wierzbicki M, Szczepaniak J, *et al*. Mechano-signalling, induced by fullerene C_{60} nanofilms, arrests the cell cycle in the G2/M phase and decreases proliferation of liver cancer cells. Int J Nanomed. 2019;14:6197. https://doi.org/10.2147/IJN.S206934.
17. Di Crescenzo A, Zara S, Di Nisio C, Ettorre V, Ventrella A, Zavan B, *et al.* Graphene oxide foils as an osteoinductive stem cell substrate. Acs Appl Bio Mater. 2019;2:1643–1651. https://doi.org/10.1021/acsabm.9b00041.
18. Chehelcheraghi F, Eimani H, Sadraie SH, Torkaman G, Amini A, Shemshadi H. Improved viability of random pattern skin flaps with the use of bone marrow mesenchymal-derived stem cells and chicken embryo extract. Iran J Basic Med Sci. 2015;18:764–772.
19. Bałaban J, Wierzbicki M, Zielińska M, Szczepaniak J, Sosnowska M, Daniluk K. Effects of Graphene Oxide Nanofilm and Chicken Embryo Muscle Extract on Muscle Progenitor Cell Differentiation and Contraction. Molecules. 2020;25:1991. https://doi.org/10.3390/molecules25081991.
20. Essid N, Chambard JC, Elgaaïed AB. Induction of epithelial-mesenchymal transition (EMT) and Gli1 expression in head and neck squamous cell carcinoma (HNSCC) spheroid cultures. Bosn J Basic Med Sci. 2018;18:336-346. https://doi.org/10.17305/bjbms.2018.3243.
21. Mu X, Sultankulov B, Agarwal R, Mahjoub A, Schott T, Greco N, *et al.* Chick embryo extract demethylates tumor suppressor genes in osteosarcoma cells. Clin Orthop Relat R. 2014;472:865-873. https://doi.org/10.1007/s11999-013-3104-6.
22. Thygesen LG, Lřkkey MM, Micklander E, Engelsen SB. Vibrational microspectroscopy of food. Raman vs. FTIR. Trends Food Sci Tech. 2003;14:50-57. https://doi.org/10.1016/S0924-2244(02)00243-1.
23. Kurantowicz N, Sawosz E, Halik G, Strojny B, Hotowy A, Grodzik M, *et al.* Toxicity studies of six types of carbon nanoparticles in a chicken-embryo model. Int J Nanomed. 2017;12:2887-2898. https://doi.org/10.2147/IJN.S131960.
24. https://www.ebi.ac.uk/pride, PRoteomics IDentifications Database, Hinxton, Cambridgeshire, UK. Identification of chicken embryo muscular and liver proteins. Available from: https://www.ebi.ac.uk/pride/archive/projects/PXD015146. Accessed June 28, 2020.

25. Iwasaki A, Sakai K, Moriya K, Sasaki T, Keene DR, Akhtar R, *et al*. Molecular mechanism responsible for fibronectin-controlled alterations in matrix stiffness in advanced chronic liver fibrogenesis. J Biol Chem. 2016;291:72-88. https://doi.org/10.1074/jbc.M115.691519.
26. Zielińska-Górska M, Hotowy A, Wierzbicki M, Bałaban J, Sosnowska M, Jaworski S, *et al*. Graphene oxide nanofilm and the addition of L-glutamine can promote development of embryonic muscle cells. J Nanobiotechnol. 2020;18:1-17. https://doi.org/10.1186/s12951-020-00636-z.
27. Fiorillo M, Verre AF, Iliut M, Peiris-Pagés M, Ozsvari B, Gandara R, *et al.* Graphene oxide selectively targets cancer stem cells, across multiple tumor types: implications for non-toxic cancer treatment, *via* "differentiation-based nano-therapy". Oncotarget. 2015;6:3553-3562. https://doi.org/10.18632/oncotarget.3348.
28. Liu Y, Wang Z, Wang X. AFM-based study of fullerenol ($C_{60}(OH)_{24}$)-induced changes of elasticity in living SMCC-7721 cells. J Mech Behav Biomed. 2015;45:65–74. https://doi.org/10.1016/j.jmbbm.2014.12.011.
29. Schrader J, Gordon-Walker TT, Aucott RL, van Deemter M, Quaas A, Walsh S, *et al.* Matrix stiffness modulates proliferation, chemotherapeutic response, and dormancy in hepatocellular carcinoma cells. Hepatology. 2011;53:1192–1205. https://doi.org/10.1002/hep.24108.
30. Kiew SF, Kiew LV, Lee HB, Imae T, Chung LY. Assessing biocompatibility of graphene oxide-based nanocarriers: a review. J Control Release. 2016;226:217-228. https://doi.org/10.1016/j.jconrel.2016.02.015.
31. Stylianopoulos T, Poh MZ, Insin N, Bawendi MG, Fukumura D, Munn LL, *et al.* Diffusion of particles in the extracellular matrix: the effect of repulsive electrostatic interactions. Biophys J. 2010;99:1342-1349. https://doi.org/10.1016/j.bpj.2010.06.016.
32. Jabaily J, Singer M. Neurotrophic and hepatotrophic stimulation of proliferation of embryonic chick muscle cells *in vitro*: assay and partial characterization of mitogenic activity in chick embryonic organ and tissue extracts. Dev Biol. 1978;64:189-202. https://doi.org/10.1016/0012-1606(78)90071-4.
33. Naba A, Clauser KR, Whittaker CA, Carr SA, Tanabe KK, Hynes RO. Extracellular matrix signatures of human primary metastatic colon cancers and their metastases to liver. BMC Cancer. 2014;14:518. https://doi.org/10.1186/1471-2407-14-518.
34. Mayoral R, Fernández-Martínez A, Boscá L, Martín-Sanz P. Prostaglandin E 2 promotes migration and adhesion in hepatocellular carcinoma cells. Carcinogenesis. 2005;26:753-761. https://doi.org/10.1093/carcin/bgi022.
35. Vernon RM, Chong PA, Tsang B, Kim TH, Bah A, Farber P, *et al.* Pi-Pi contacts are an overlooked protein feature relevant to phase separation. Elife. 2018;7: https://doi.org/10.7554/eLife.31486.
36. Xie H, Cao T, Franco-Obregón A, Rosa V. Graphene-induced osteogenic differentiation is mediated by the integrin/FAK axis. Int J Mol Sci. 2019;20:574. https://doi.org/10.3390/ijms20030574.
37. Kopova I, Bacakova L, Lavrentiev V, Vacik J. Growth and potential damage of human bone-derived cells on fresh and aged fullerene C_{60} Int J Mol Sci. 2013;14:9182-9204.

https://doi.org/10.1371/journal.pone.0123680.

38. McCallion C, Burthem J, Rees-Unwin K, Golovanov A, Pluen A. Graphene in therapeutics delivery: Problems, solutions and future opportunities. Eur J Pharm Biopharm. 2016;104:235-250. https://doi.org/10.1016/j.ejpb.2016.04.015.
39. Albanese A, Walkey CD, Olsen JB, Guo H, Emili A, Chan WCW. Secreted biomolecules alter the biological identity and cellular interactions of nanoparticles. Acs Nano. 2014;8:5515-5526. https://doi.org/10.1021/nn4061012.
40. Fu Y, Fang Z, Liang Y, Zhu X, Prins P, Li Z, *et al*. Overexpression of integrin β1 inhibits proliferation of hepatocellular carcinoma cell SMMC-7721 through preventing Skp2-dependent degradation of p27 *via* PI3K pathway. J Cell Biochem. 2007;102:704-718. https://doi.org/10.1002/jcb.21323.
41. Wang K, Ruan J, Song H, Zhang J, Wo Y, Guo S, *et al.* Biocompatibility of graphene oxide. Nanoscale Res Lett. 2011;6:8. https://doi.org/10.1007/s11671-010-9751-6.
42. Humphries JD, Byron A, Humphries MJ. Integrin ligands at a glance. J Cell Sci. 2006;119: 3901-3903. https://doi.org/10.1242/jcs.03098.
43. Arun AS, Tepper CG, Lam KS. Identification of integrin drug targets for 17 solid tumor types. Oncotarget. 2018;9:30146-30162. https://doi.org/10.18632/oncotarget.25731.
44. Cheng B, Wan W, Huang G, Li Y, Genin GM, Mofrad MRK, *et al*. Nanoscale integrin cluster dynamics controls cellular mechanosensing via FAKY397 phosphorylation. Science Advance. 2020;6:eaax1909. https://doi.org/10.1126/sciadv.aax1909.
45. Marchesan S, Melchionna M, Prato M. Carbon nanostructures for nanomedicine: opportunities and challenges. Fuller Nanotub Car N. 2014;22:190–195. https://doi.org/10.1080/1536383X.2013.798726.
46. Nguyen VH, Meghani NM, Amin HH, Tran TTD, Tran PHL, Park C, *et al.* Modulation of serum albumin protein corona for exploring cellular behaviors of fattigation-platform nanoparticles. Colloid Surface B. 2018;170:179–186. https://doi.org/10.1016/j.colsurfb.2018.05.060.
47. Wu S, Zheng Q, Xing X, Dong Y, Wang Y, You Y, *et al*. Matrix stiffness-upregulated LOXL2 promotes fibronectin production, MMP9 and CXCL12 expression and BMDCs recruitment to assist pre-metastatic niche formation. J Exp Clin Cancer Res. 2018;37:99. https://doi.org/10.1186/s13046-018-0761-z.
48. Alday-Parejo B, Stupp R, Rüegg C. Are integrins still practicable targets for anti-cancer therapy? Cancers. 2019;11:978. https://doi.org/10.3390/cancers11070978.
49. Yu J, Zhang C, Yu Q, Yu H, Zhang B. ADAR1 p110 enhances adhesion of tumor cells to extracellular matrix in hepatocellular carcinoma *via* up-regulating ITGA2 expression. Med Sci Monit. 2019;25:1469-1479. https://doi.org/10.12659/MSM.911944.
50. Koivunen E, Wang B, Ruoslahti E. Isolation of a highly specific ligand for the as/3t integrin from a phage display library. J Cell Biol. 1994;124:373-380. https://doi.org/10.1083/jcb.124.3.373.
51. Zhu J, Xu M, Gao M, Zhang Z, Xu Y, Xia T, *et al.* Graphene oxide induced perturbation to plasma membrane and cytoskeletal meshwork sensitize cancer cells to chemotherapeutic agents. Acs Nano.

2017;11:2637-2651. https://doi.org/10.1021/acsnano.6b07311.

52. Lasocka I, Jastrzębska E, Szulc-Dąbrowska L, Skibniewski M, Pasternak I, Hubalek Kalbacova M, *et al.* The effects of graphene and mesenchymal stem cells in cutaneous wound healing and their putative action mechanism. Int J Nanomed. 2019;14: 2281-2299. https://doi.org/10.2147/IJN.S190928.
53. Cance WG, Harris JE, Iacocca MV, Roche E, Yang X, Chang J, *et al.* Immunohistochemical analyses of focal adhesion kinase expression in benign and malignant human breast and colon tissues: correlation with preinvasive and invasive phenotypes. Clin Cancer Res. 2000;6:2417-2423.
54. Shang N, Wang H, Bank T, Perera A, Joyce C, Kuffel G, *et al.* Focal adhesion kinase and β-catenin cooperate to induce hepatocellular carcinoma. Hepatology. 2019;70:1631-1645. https://doi.org/10.1002/hep.30707.
55. Ren K, Lu X, Yao N, Chen Y, Yang A, Chen H, *et al.* Focal adhesion kinase overexpression and its impact on human osteosarcoma. 2015;6:31085-31103. https://doi.org/10.18632/oncotarget.5044.
56. Bai XM, Zhang W, Liu NB, Jiang H, Lou KX, Peng T, *et al.* Focal adhesion kinase: important to prostaglandin E2-mediated adhesion, migration and invasion in hepatocellular carcinoma cells. Oncol Rep. 2009;21:129-136. https://doi.org/10.3892/or_00000199.
57. Mui KL, Chen CS, Assoian RK. The mechanical regulation of integrin–cadherin crosstalk organizes cells, signaling and forces. J Cell Sci. 2016;129:1093-1100. https://doi.org/10.1242/jcs.183699.
58. Zhang X, Yang M, Shi H, Hu J, Wang Y, Sun Z, *et al.* Reduced E-cadherin facilitates renal cell carcinoma progression by WNT/β-catenin signaling activation. Oncotarget. 2017;8: 19566–19576. https://doi.org/10.18632/oncotarget.15361.
59. Kasprzak A, Rogacki K, Adamek A, Sterzyńska K, Przybyszewska W, Seraszek-Jaros A, *et al.* Tissue expression of β-catenin and E- and N-cadherins in chronic hepatitis C and hepatocellular carcinoma. Arch Med Sci. 2017;13: 1269–1280. https://doi.org/10.5114/aoms.2017.65272.
60. Luo Y, Ren Z, Du B, Xing S, Huang S, Li Y, *et al.* Structure identification of viceninII extracted from *Dendrobium officinale* and the reversal of TGF-β1-induced epithelial□mesenchymal transition in lung adenocarcinoma cells through TGF-β/Smad and PI3K/Akt/mTOR signaling pathways. Molecules. 2019;24:144. https://doi.org/10.3390/molecules24010144.
61. Kurantowicz N, Strojny B, Sawosz E, Jaworski S, Kutwin M, Grodzik M, *et al.* Biodistribution of a high dose of diamond, graphite, and graphene oxide nanoparticles after multiple intraperitoneal injections in rats. Nanoscale Res Lett. 2015;10:398. https://doi.org/10.1186/s11671-015-1107-9.
62. Strojny B, Kurantowicz N, Sawosz E, Grodzik M, Jaworski S, Kutwin M, *et al.* Long term influence of carbon nanoparticles on health and liver status in rats. PloS One. 2015;10:e0144821. https://doi.org/10.1371/journal.pone.0144821.
63. Szmidt M, Sawosz E, Urbańska K, Jaworski S, Kutwin M, Hotowy A, *et al.* Toxicity of different forms of graphene in a chicken embryo model. Environ Sci Pollut Res Int. 2016;23:19940-19948. https://doi.org/10.1007/s11356-016-7178-z.

64. Haeger A, Krause M, Wolf K, Friedl P. Cell jamming: collective invasion of mesenchymal tumor cells imposed by tissue confinement. Biochim Biophys Acta. 2014;1840:2386–2395. doi:10.1016/j.bbagen.2014.03.020.
65. Cucina A, Biava PM, D'Anselmi F, Coluccia P, Conti F, di Clemente R, *et al.* Zebrafish embryo proteins induce apoptosis in human colon cancer cells (Caco2). Apoptosis. 2006;11:1617-1628. https://doi.org/10.1007/s10495-006-8895-4.
66. Allegrucci C, Rushton MD, Dixon JE, Sottile V, Shah M, Kumari R, *et al.* Epigenetic reprogramming of breast cancer cells with oocyte extracts. Mol Cancer. 2011;10:7. https://doi.org/10.1186/1476-4598-10-7.
67. Wang Y, Shenouda S, Baranwal S, Rathinam R, Jain P, Bao L, *et al.* Integrin subunits alpha5 and alpha6 regulate cell cycle by modulating the chk1 and Rb/E2F pathways to affect breast cancer metastasis. Mol Cancer. 2011;10:1-11. https://doi.org/10.1186/1476-4598-10-84.
68. Moreno-Layseca P, Streuli CH. Signalling pathways linking integrins with cell cycle progression. Matrix Biol. 2014;34:144-153. https://doi.org/10.1016/j.matbio.2013.10.011.
69. Yin L, Chang C, Xu C. G2/M checkpoint plays a vital role at the early stage of HCC by analysis of key pathways and genes. Oncotarget. 2017;8:76305-76317. https://doi.org/10.18632/oncotarget.19351.
70. Lin CH, Chung MY, Chen WB, Chien CH. Growth inhibitory effect of the human *NIT2* gene and its allelic imbalance in cancers. Febs J. 2007;274:2946-2956. https://doi.org/10.1111/j.1742-4658.2007.05828.x.
71. Lee K, Suzuki H, Aiso S, Matsuoka M. Overexpression of TDP-43 causes partially p53-dependent G2/M arrest and p53-independent cell death in HeLa cells. Neurosci Lett. 2012;506:271-276. https://doi.org/10.1016/j.neulet.2011.11.021.
72. Sawosz E, Grodzik M, Hotowy A, Sosnowska M, Urbanowska B, Szczepaniak J, *et al.* Warsaw University of Life Sciences. The method of multilateral assessment of biocompatibility of materials. Poland patent 423414. 2017 Nov 10.
73. Cox J, Mann M. MaxQuant enables high peptide identification rates, individualized p.p.b.-range mass accuracies and proteome-wide protein quantification. Nat Biotechnol. 2008;26:1367-1372. https://doi.org/10.1038/nbt.1511.
74. Tyanova S, Temu T, Carlson A, Sinitcyn P, Mann M, Cox J. Visualization of LC-MS/MS proteomics data in MaxQuant. Proteomics. 2015;15:1453-1456. https://doi.org/10.1002/pmic.201400449.
75. https://medschool.ucsd.edu, UC San Diego, Health Sciences, California, USA. Cell cycle analysis by DNA content (propidium iodide) [accessed Jul 17, 2018]. Available from URL: https://healthsciences.ucsd.edu/research/moores/shared-resources/flow-cytometry/protocols/Pages/cell-cycle-with-pi.aspx.
76. Szczepaniak J, Strojny B, Sawosz Chwalibog E, Jaworski S, Jagiello J, Winkowska M, *et al.* Effects of reduced graphene oxides on apoptosis and cell cycle of glioblastoma multiforme. Int J Mol Sci. 2018;19:3939. https://doi.org/10.3390/ijms19123939.

77. Dingemans AM, van den Boogaart V, Vosse BA, van Suylen RJ, Griffioen AW, Thijssen VL. Integrin expression profiling identifies integrin alpha5 and beta1 as prognostic factors in early stage non-small cell lung cancer. Mol Cancer. 2010;9:152. https://doi.org/10.1186/1476-4598-9-152.
78. Chen TC, Lai CH, Chang JL, Chang SW. Mitomycin C retardation of corneal fibroblast migration *via* sustained dephosphorylation of paxillin at tyrosine 118. Invest Ophth Vis Sci. 2012;53:1539-1547. https://doi.org/10.1167/iovs.11-9203.

Figures

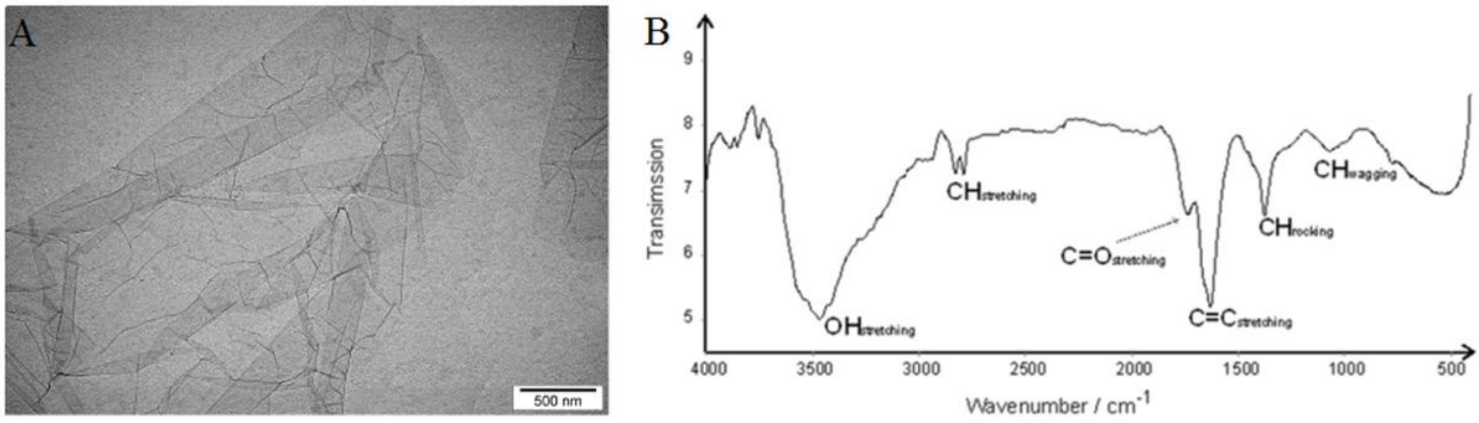

Figure 1

Characterisation of graphene oxide flakes. (A) Transmission electron microscopy image of graphene oxide. Scale bar: 500 nm. (B) Fourier transform infrared spectrum of graphene oxide in the middle region (4000 – 500 cm−1).

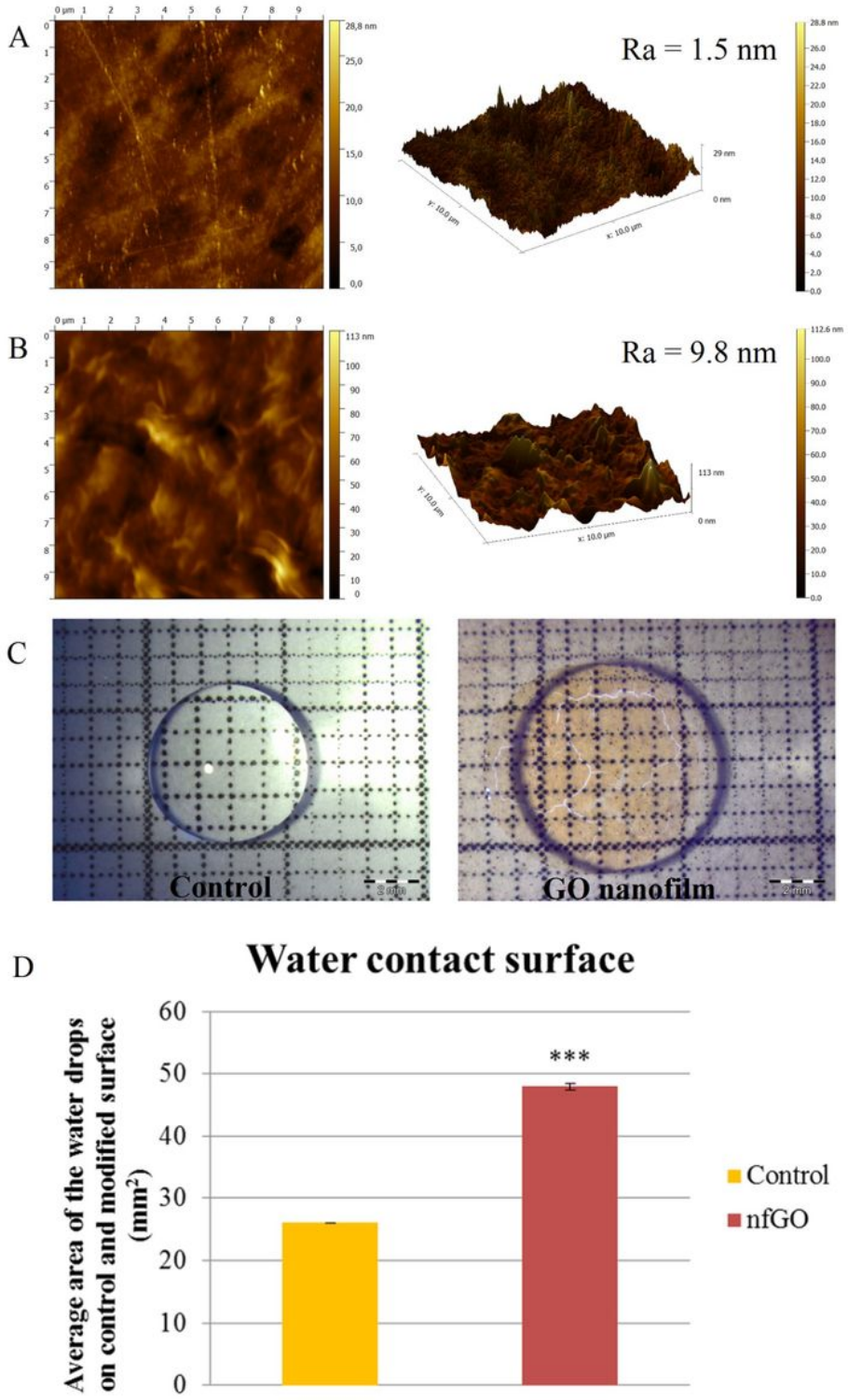

Figure 2

Characterisation of graphene oxide nanofilm. Topographical image of the uncoated (A; scale bar: 10 µm x 10 µm x 29 nm) and graphene oxide-coated plate (B; scale bar: 10 µm x 10 µm x 113 nm). Left side: face surface. Right side: three-dimensional atomic force microscopy image. Ra: roughness average (C) Visualisation of the hydrophilicity properties of graphene oxide nanofilm in relation to the plastic plate surface. Left side: water contact surface on Petri dish. Right side: water contact surface on Petri dish

coated with GO nanofilm. Scale bar 2 mm. (D) Comparison of water drop area on clean polystyrene surface and polystyrene surface coated with nfGO using ImageJ.

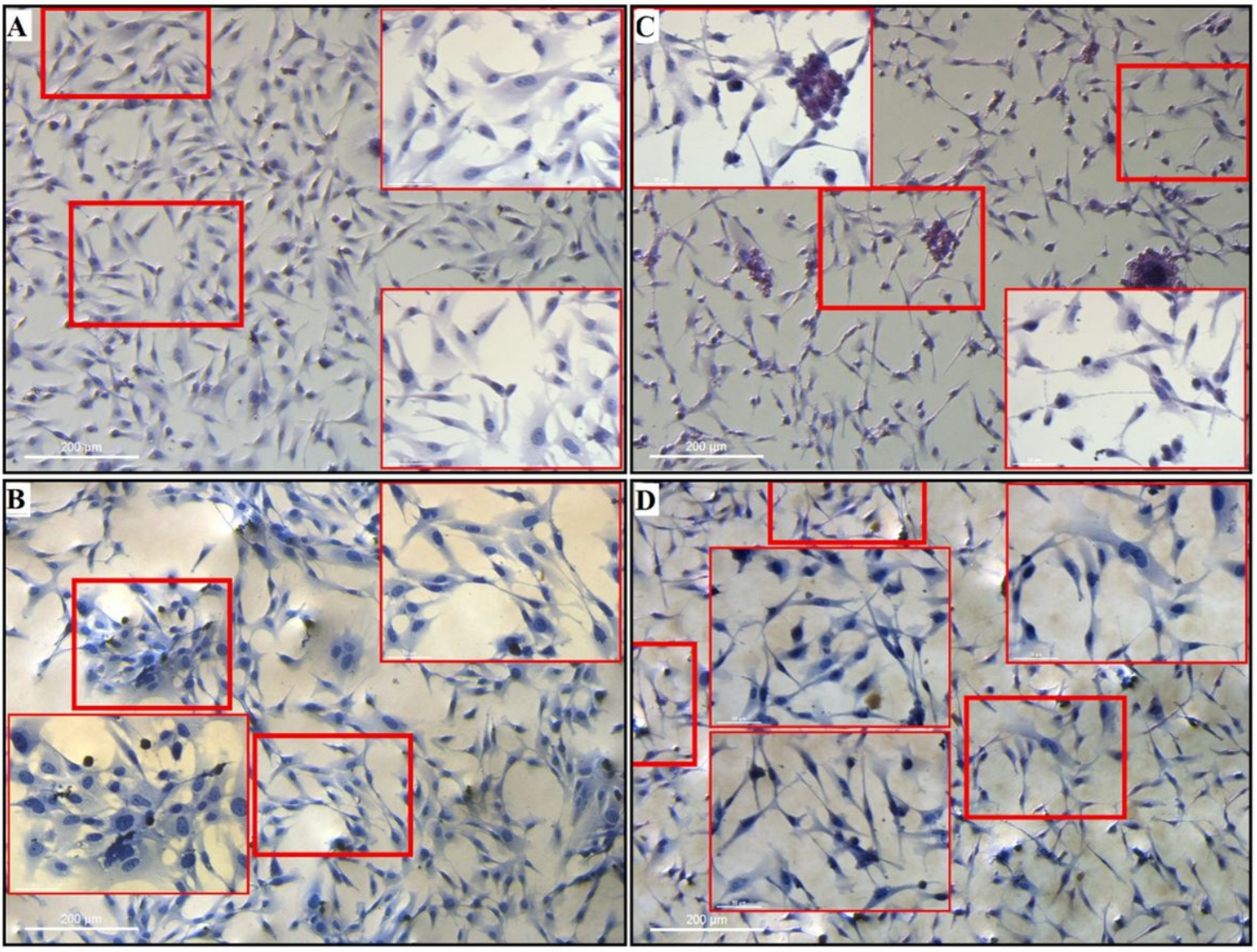

Figure 3

HS-5 cell morphology after 48 hours of culture using H&E staining (A) control (B) cultured on graphene oxide nanofilm (nfGO), (C) cultured with the addition of chicken embryo liver extract (CELE) (D) cultured on graphene oxide nanofilm with the addition of chicken embryo liver extract (nfGO + CELE). Light optical microscopy. The greater red frames (scale bar: 50 µm) indicate magnified parts of the main pictures (marked by smaller red frames, scale bar: 200 µm).

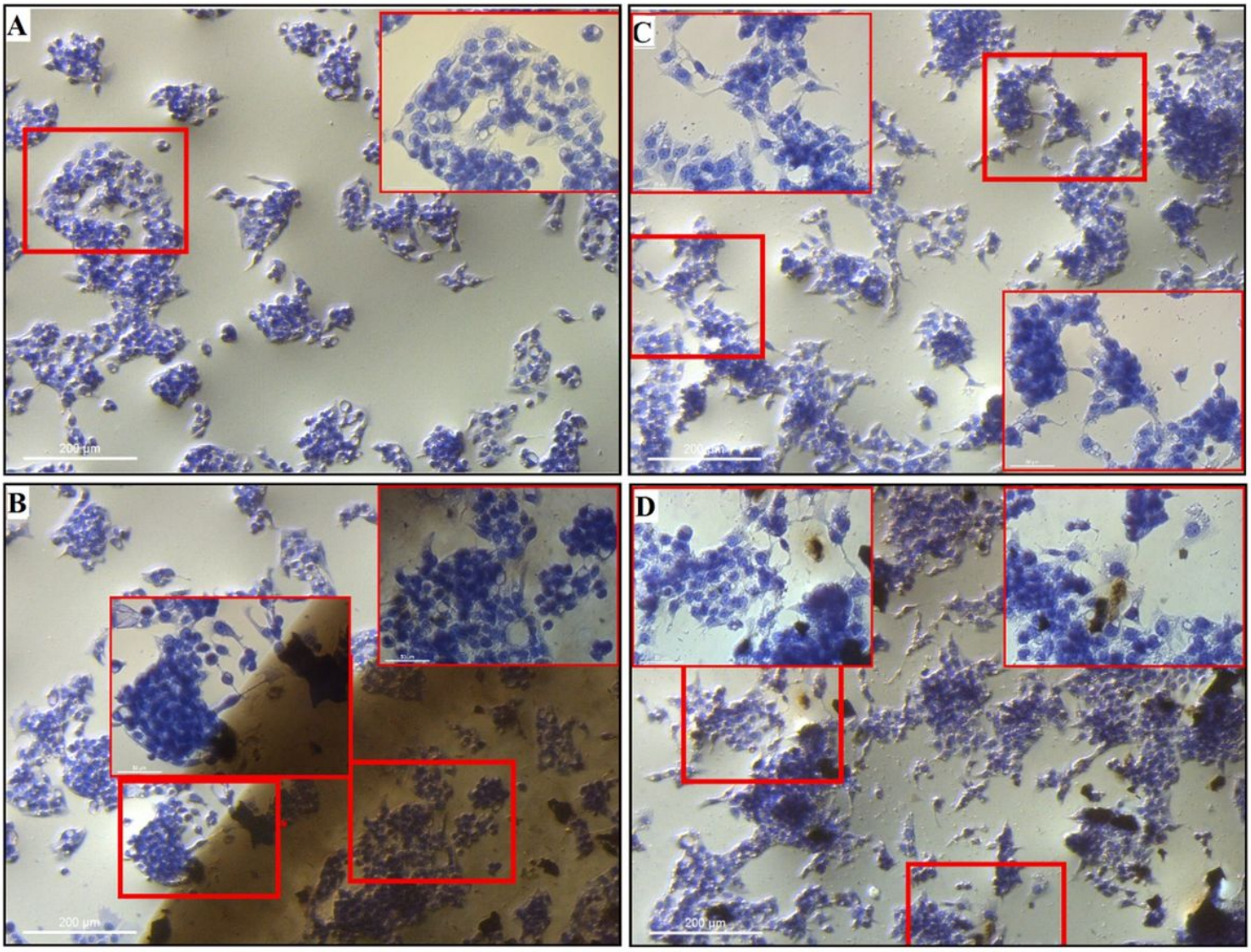

Figure 4

HepG2 cell morphology after 48 hours of culture using H&E staining (A) control (B) cultured on graphene oxide nanofilm (nfGO), (C) cultured with the addition of chicken embryo liver extract (CELE) (D) cultured on graphene oxide nanofilm with the addition of chicken embryo liver extract (nfGO + CELE). Light optical microscopy. The greater red frames (scale bar: 50 µm) indicate magnified parts of the main pictures (marked by smaller red frames, scale bar: 200 µm).

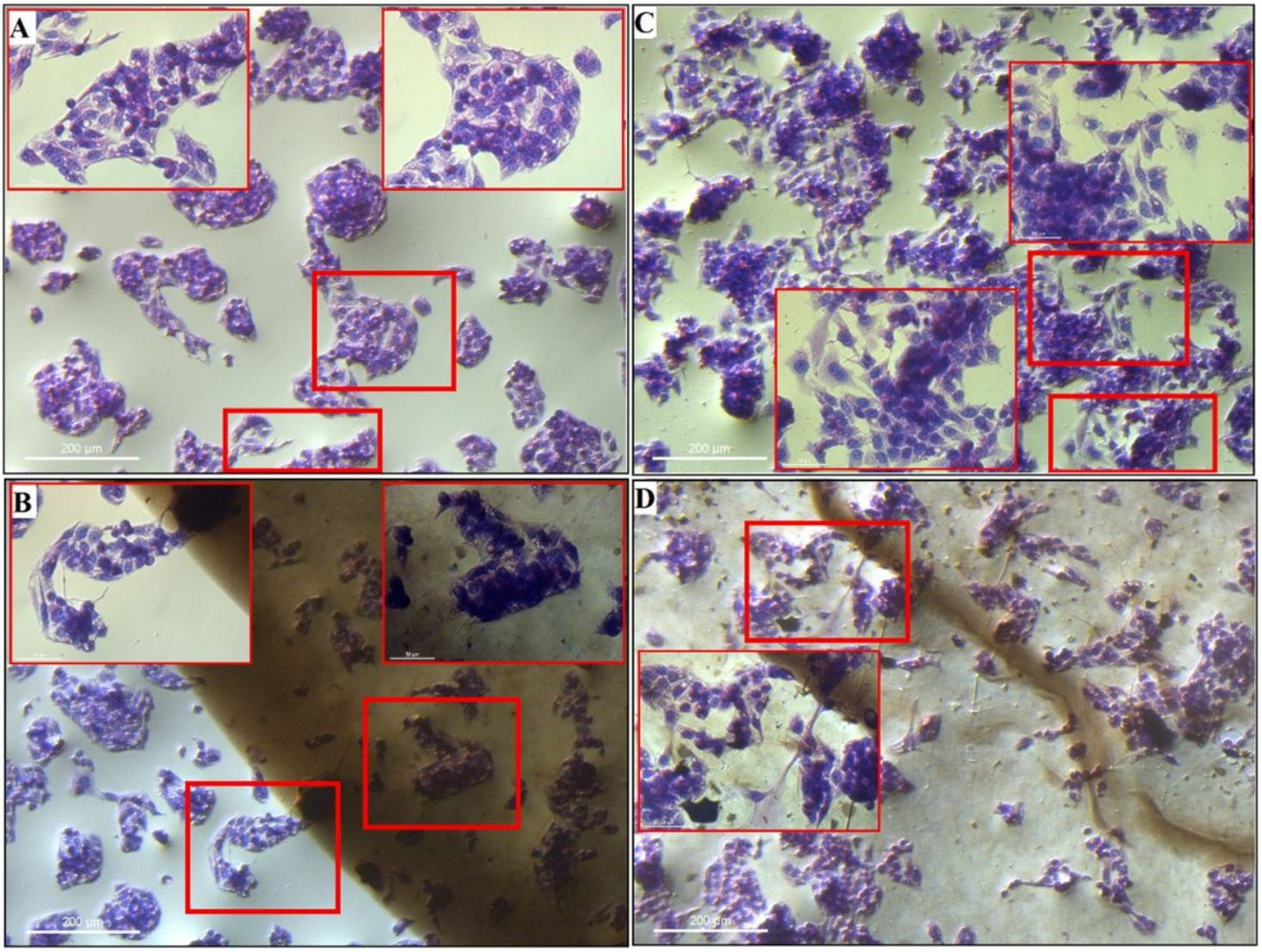

Figure 5

C3A cell morphology after 48 hours of culture using H&E staining (A) control (B) cultured on graphene oxide nanofilm (nfGO), (C) cultured with the addition of chicken embryo liver extract (CELE), (D) cultured on graphene oxide nanofilm with the addition of chicken embryo liver extract (nfGO + CELE). Light optical microscopy. The greater red frames (scale bar: 50 µm) indicate magnified parts of the main pictures (marked by smaller red frames, scale bar: 200 µm).

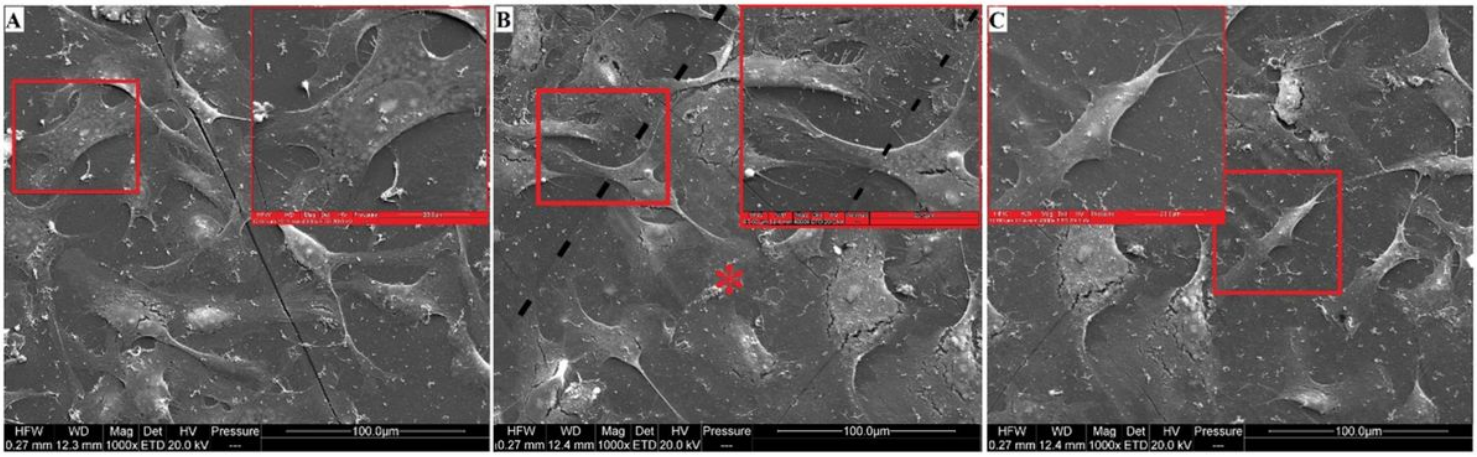

Figure 6

HS-5 cell morphology by scanning electron microscopy after 7 days of culture. (A) cultured on standard polystyrene plate, (B) cultured on graphene oxide nanofilm (nfGO) partly covering a standard polystyrene plate (red asterisk), (C) cultured on graphene oxide nanofilm (nfGO). Black dotted line indicates the border between the polystyrene and GO surface. The greater red frames (scale bar: 20 µm) indicate magnified parts of the main pictures (marked by smaller red frames, scale bar: 100 µm).

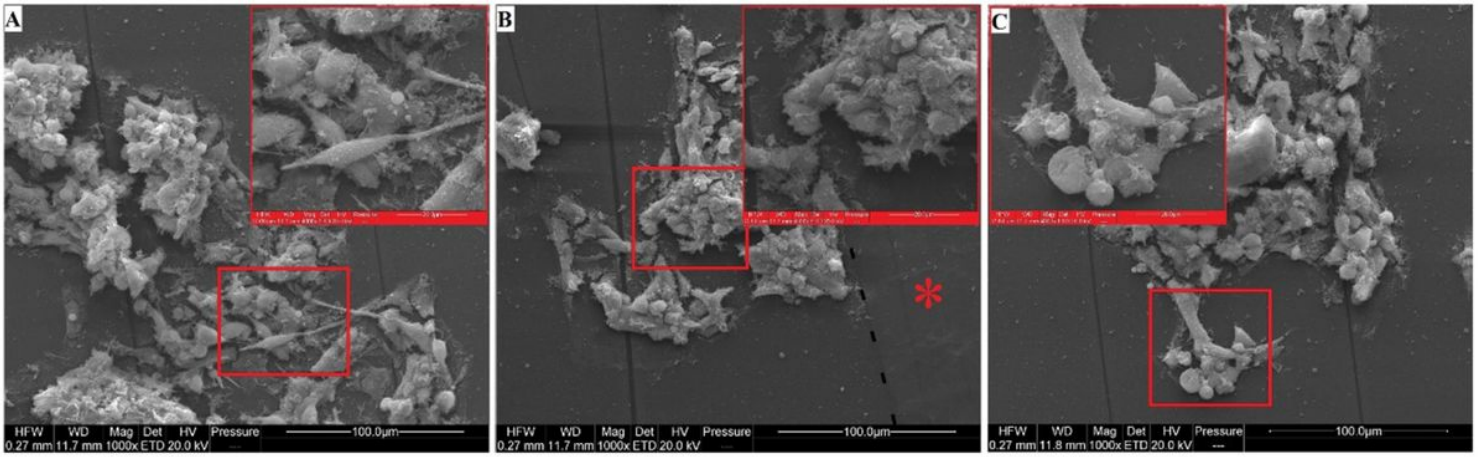

Figure 7

HepG2 cell morphology after 7 days by scanning electron microscope. (A) cultured on standard polystyrene plate, (B) cultured on graphene oxide nanofilm (nfGO) partly covering a standard polystyrene plate (red asterisk), (C) cultured on graphene oxide nanofilm (nfGO). Black dotted line indicates the border between polystyrene and GO surface. The greater red frames (scale bar: 20 µm) indicate magnified parts of the main pictures (marked by smaller red frames, scale bar: 100 µm).

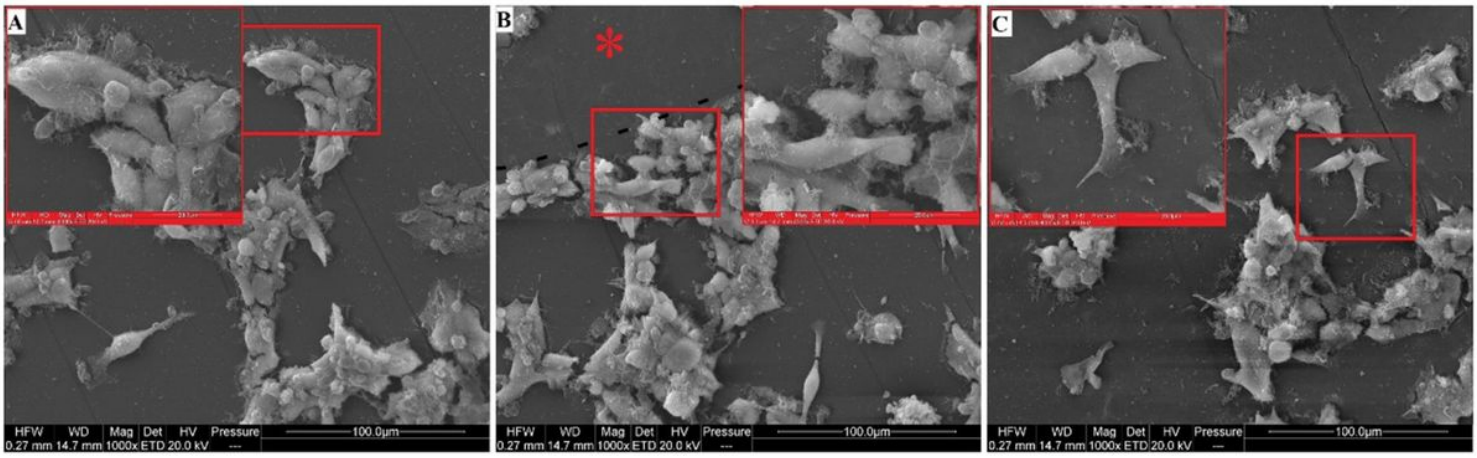

Figure 8

C3A cell morphology after 7 days of culture by scanning electron microscope. (A) cultured on standard polystyrene plate, (B) cultured on graphene oxide nanofilm (nfGO) partly covering a standard polystyrene plate (red asterisk), (C) cultured on graphene oxide nanofilm (nfGO). Black dotted line indicates the border between polystyrene and GO surface. The greater red frames (scale bar: 20 µm) indicate magnified parts of the main pictures (marked by smaller red frames, scale bar: 100 µm).

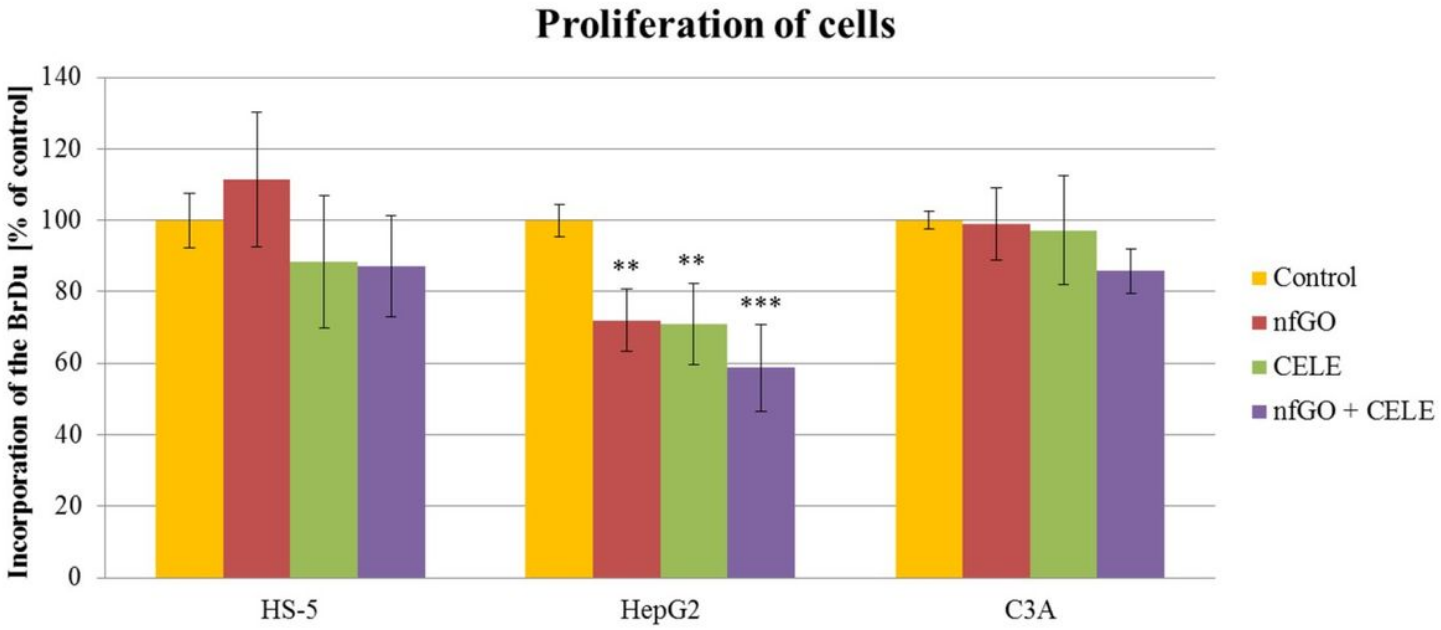

Figure 9

Analysis of HS-5, HepG2 and C3A cell proliferation after 48h of cultivation using BrdU test. Cells were cultured on graphene oxide nanofilm (nfGO), cultured with the addition of chicken embryo liver extract (CELE), and cultured on graphene oxide nanofilm with the addition of chicken embryo liver extract (nfGO + CELE).

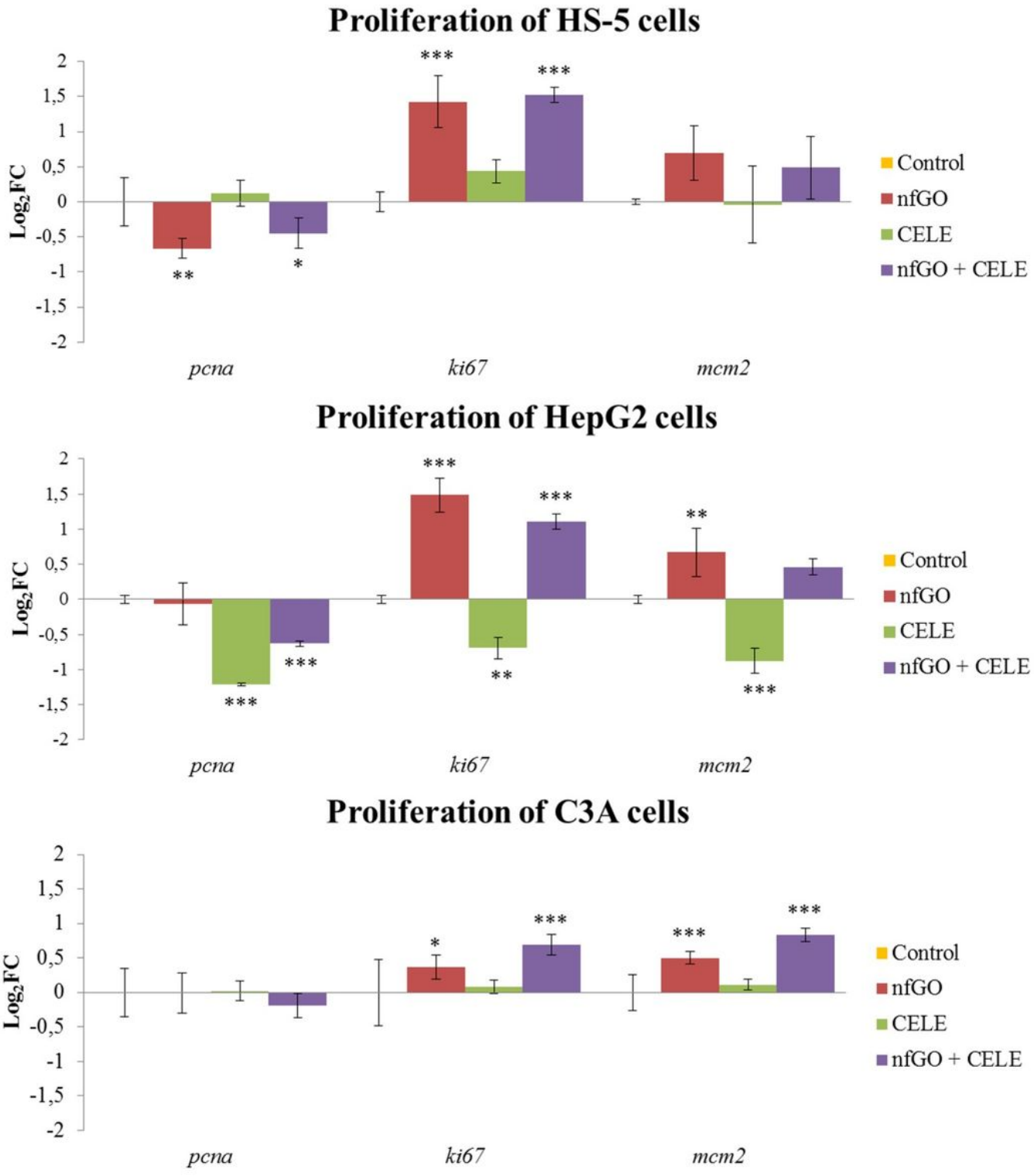

Figure 10

Expression of genes pcna, ki67, and mcm2 at the mRNA level in HS-5, HepG2 and C3A cells after 7 days of cultivation on graphene oxide nanofilm (nfGO), cultivation with the addition of chicken embryo liver extract (CELE), and cultivation on graphene oxide nanofilm with addition of chicken embryo liver extract (nfGO + CELE) using RT-PCR. Bars represent the means with SD (n = 4). Relative expression was calculated using the gapdh gene. The results are presented as log2FC values, and untreated cells are

depicted as 0. Values above/below 0 indicate upregulation/downregulation of gene expression. Abbreviations: FC, fold change.

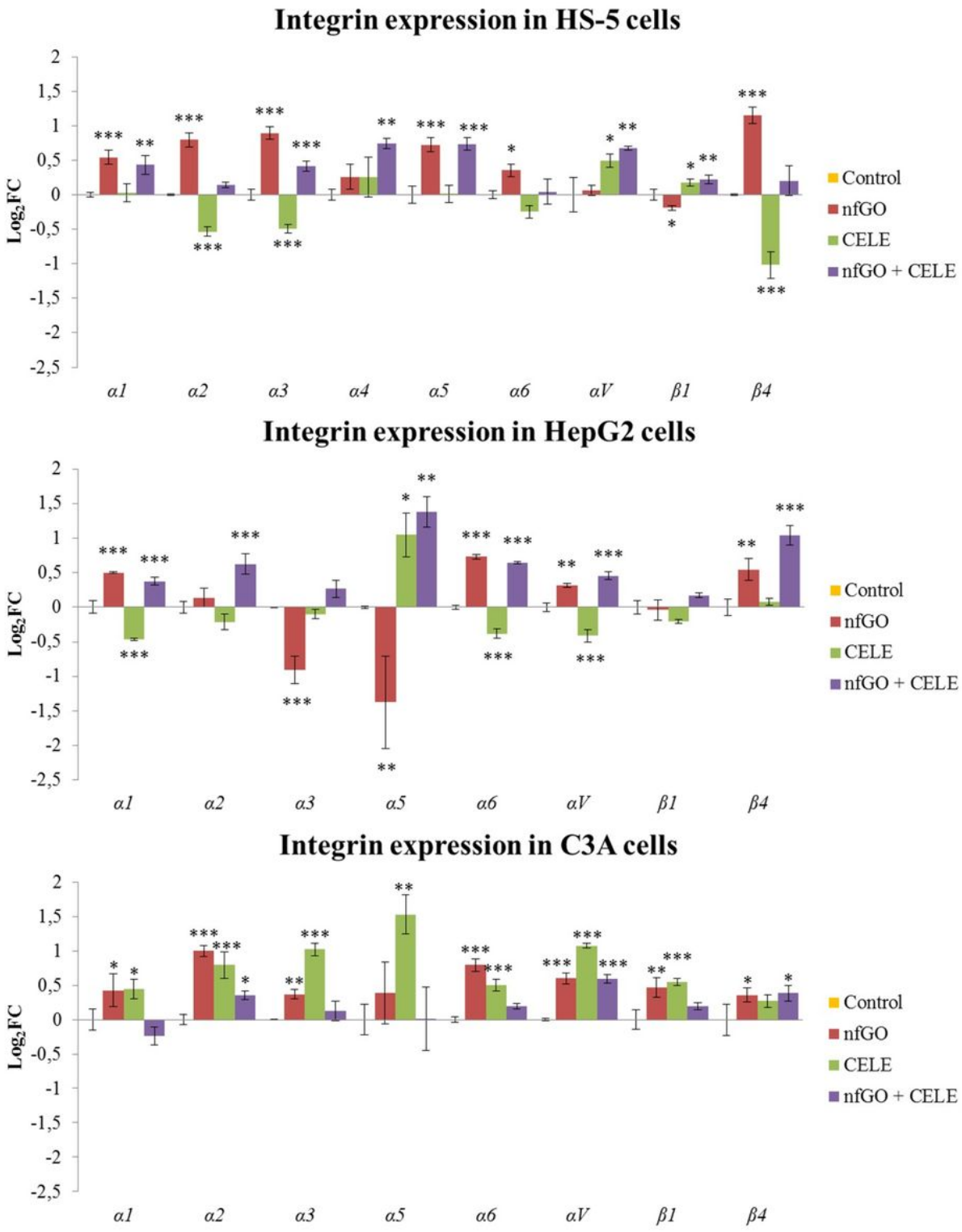

Figure 11

Expression of genes integrin at the mRNA level in HS-5, HepG2, and C3A cells after 7 days of cultivation on graphene oxide nanofilm (nfGO), cultivation with addition of chicken embryo liver extract (CELE), and cultivation on graphene oxide nanofilm with addition of chicken embryo liver extract (nfGO + CELE) using

RT-PCR. Bars represents the means with SD (n = 4). Relative expression was calculated using the gapdh gene. The results are presented as log2FC values, and untreated cells are depicted as 0. Values above/below 0 indicate upregulation/downregulation of gene expression. Abbreviations: FC, fold change.

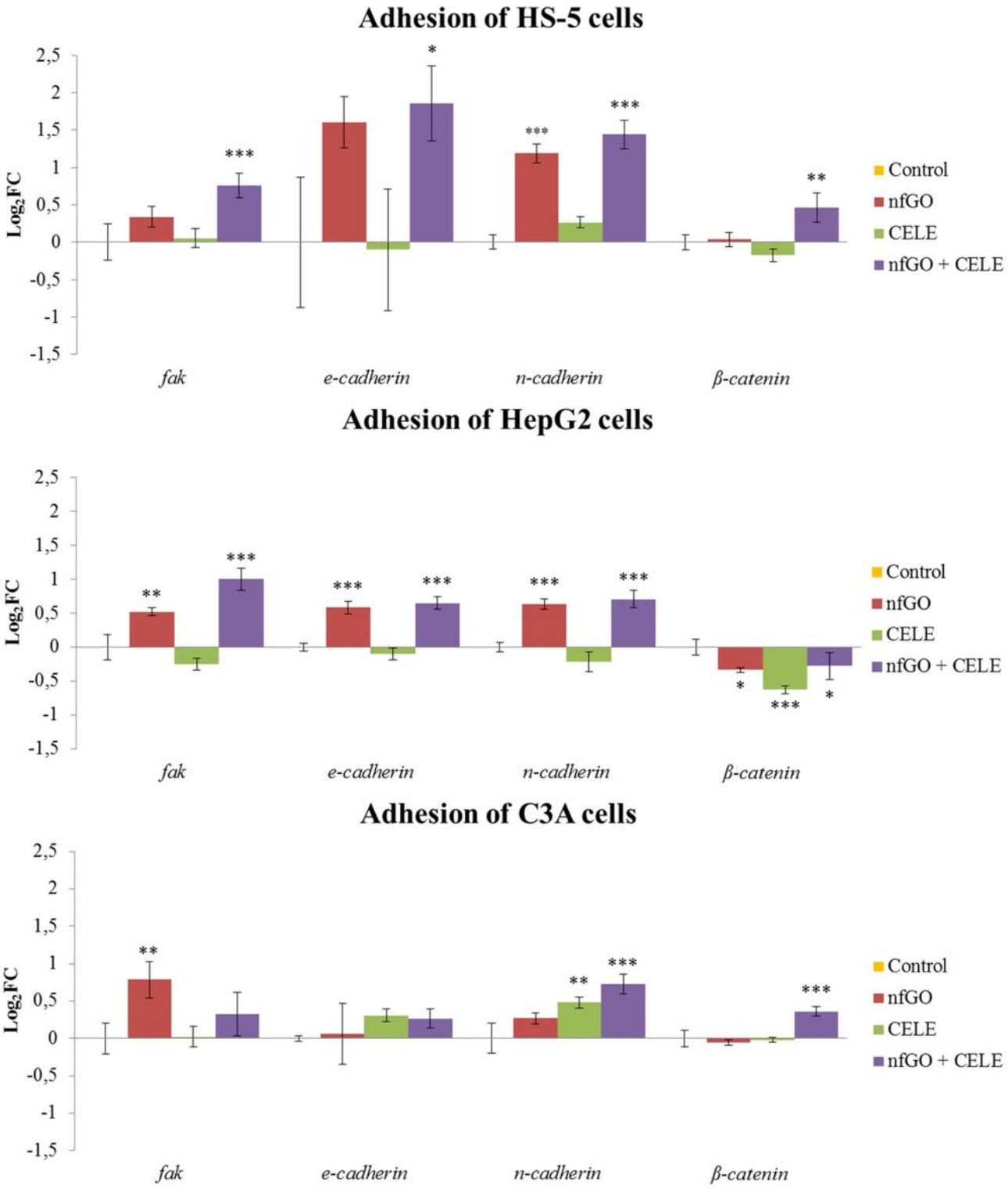

Figure 12

Expression of genes focal adhesion kinase (fak), e-cadherin, n-cadherin and β-catenin genes at the mRNA level in HS-5, HepG2 and C3A cells after 7 days of cultivation on graphene oxide nanofilm (nfGO), with

addition of chicken embryo liver extract (CELE), and on graphene oxide nanofilm with addition of chicken embryo liver extract (nfGO + CELE) using RT-PCR. Bars represents the means with SD (n = 4). Relative expression was calculated using the gapdh gene. The results are presented as log2FC values, and untreated cells are depicted as 0. Values above/below 0 indicate upregulation/downregulation of gene expression. Abbreviations: FC, fold change.

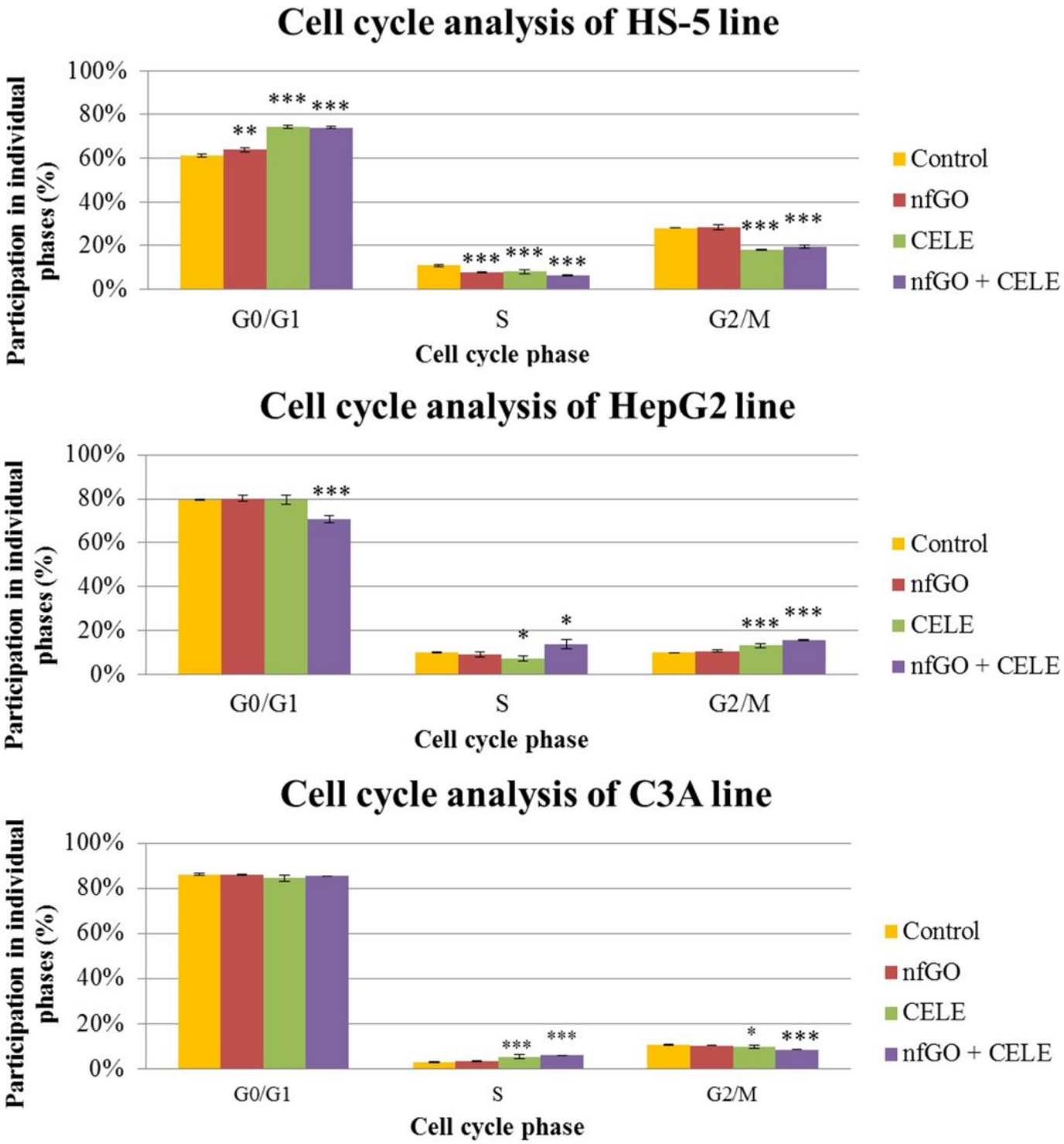

Figure 13

Effect of graphene oxide nanofilm (nfGO), chicken embryo liver extract (CELE), and graphene oxide nanofilm with addition of chicken embryo liver extract (nfGO + CELE) on the number (percentage) of HS-5, HepG2, and C3A cells in G0/G1, S, and G2/M phases. Cell cycle analysis was performed using propidium iodide (PI) 488 assay.

Supplementary Files

This is a list of supplementary files associated with this preprint. Click to download.

- image.jpg
- Additionalfile1.docx